Noise Resistant Control Charts for Detecting Periodicity from Correlation

Yongxiang Li, Yunji Zhang

Department of Industrial Engineering and Management, Shanghai Jiao Tong University

Qian Xiao*

Department of Statistics, University of Georgia

Jianguo Wu

Department of Industrial Engineering and Management, Peking University

Abstract

Control charts are widely used to detect process variations that can reveal out-of-control events. Among various methods in the literature, spectral control charts are popular for monitoring processes with periodic behavior. Yet, in highly noisy environments, their performance may become unsatisfactory, because they are designed on the spectral features (e.g., periodogram) which could be easily masked by strong noise. Moreover, they would incorrectly report many correlated-but-not-periodic signals as periodic ones, leading to a high false discovery rate. To address these issues, we develop a new noise resistant feature in the time domain, based on which we propose two robust tests and establish noise resistant control charts for detecting periodicity from correlation. Our developed feature is proved to have appealing finite-sample and asymptotic properties. Additionally, we develop an efficient computation for calculating the proposed test statistics. Simulations and case studies are presented to demonstrate the superiority of the proposed approach compared to some state-of-the-art methods.

*Contact: Qian Xiao, qian.xiao@uga.edu, Department of Statistics, University of Georgia, Athens, GA, USA, 30602.

1   Introduction

Periodic behaviors are observed in many processes, which indicate out-of-control conditions in some applications (McSweeney, 2006b). For example, monitoring the periodicity in products of a manufacturing process, such as the paper production process (McSweeney, 2006a), can reveal whether cyclic fluctuations exist in the products (Tatum, 1996). The detection of periodicity in the vibration signals collected from rotating machines indicates the failure of critical components, such as bearings or gears (Fan et al., 2018). Additionally, if we can quickly identify that a process is periodic, the detected periodicity can then be exploited to further improve the performance of many applications (Genton and Hall, 2007; Li et al., 2021; Cerovecki et al., 2022). Thus, periodicity detection and monitoring are of great importance.

Control charts are a fundamental tool in statistical process control (SPC) for monitoring the stability and performance of a process over time. Popular control charts include the Shewhart chart (Shewhart, 1931), the exponentially weighted moving average (EMWA) chart (Roberts, 1959; Zhang et al., 2023; Zou et al., 2024), and the cumulative sum (CUSUM) chart (Page, 1954; Austin et al., 2024; Zheng et al., 2024), which are widely used to detect changes in the process mean. Multivariate control charts, e.g., the Hotelling T^2 chart (Hotelling, 1947; Li et al., 2018), are also used for process control and monitoring. A review of recent advances in SPC can be found in Shi (2006); Qiu (2014); Colosimo et al. (2024). However, most conventional control charts may not be able to detect periodic behavior (Beneke et al., 1988).

Some spectral control charts (Bølviken, 1983; Beneke et al., 1988; Zhao-Guo, 1988; Spurrier and Thombs, 1990; Tatum, 1996; Hurd and Gerr, 1991) have been proposed for

detecting the onset of periodic behaviors (i.e., out-of-control behaviors). Current spectral methods are often designed on the features (such as periodogram) in the frequency domain via the fast Fourier transform. Yet, they are vulnerable to the masking effect of strong noise, and thus are not effective in detecting the periodicity in noisy environments; see Fig. 1 in the next section for an illustrative example.

In addition to the control charts designed for detecting periodicity, various tests have been proposed for serial correlation (Hong, 1996; Qiu et al., 2020; Xie and Qiu, 2024). However, both categories of methods encounter challenges in effectively discriminating between periodic and correlated-but-not-periodic (CBNP) signals. Specifically, in this work, we focus on a common type of CBNP signals that are generated from stationary Gaussian processes (GPs). Current tests for serial correlation fall short in further distinguishing periodic and CBNP signals, while spectral control charts often assume the test signals to be either white Gaussian noise or periodic. Moreover, many applications involve temporally correlated signals that current spectral control charts would mistakenly report them as periodic (leading to false periodicity alarms). Therefore, new control charts that can effectively discriminate periodic signals from white Gaussian noise and CBNP signals are needed in practice, particularly for the cases subject to strong noise.

To overcome the masking effect of strong noise, we develop a new feature in the time domain, called the enhanced noise resistant correlation (EnNRC), which provides the maximum correlation value if and only if the signals are periodic and the segmentation is correctly specified. When the signals are white Gaussian noise (i.e., under the null hypothesis of the proposed test), the EnNRC features asymptotically follow a multivariate normal distribution, and their (asymptotic) covariance matrix is positive definite. In addition, we develop an efficient approach for calculating its covariance matrix, which has a reduced time complexity of $\mathcal{O}\left(p^2 l\right)$, where p and l are the number of inspection periods and the signal length respectively and $p << l$. Compared to the classic noise resistant correlation (NRC; Fan et al., 2018), which drops the last segment of signals, the proposed EnNRC has

two overwhelming advantages. First, it employs a new segmentation strategy and considers all signal points. Thus, it does not suffer from unnecessary information loss. Second, it has appealing finite-sample and asymptotic properties, as shown in Section 3, which cannot be found in NRC (Fan et al., 2018).

Based on the developed EnNRC feature, we propose two novel tests, the maximum order (MO) test and a new T^2 test, to effectively discriminate periodic signals, CBNP signals (generated by GPs), and white Gaussian noise. The proposed MO test is developed for robust detection of periodicity in noisy environments, whose test statistic is the maximum value of the orthogonal transformations of EnNRC. Such a feature is identically and independently distributed under the null hypothesis, and the cumulative distribution of the MO statistic has a closed form, making the test analytically tractable. Notably, when the signals are CBNP, many conventional hypothesis tests, e.g., Fisher's test (Fisher, 1929), tend to reject its null hypothesis and incorrectly identify the CBNP signals as periodic, while the MO test is unlikely to reject its null hypothesis and thus can draw the correct conclusion, because the nonperiodic correlation in the CBNP signals has nearly no impact on the maximum value of our developed features. Empirical studies in this paper verify the superiority of the proposed MO test for detecting the presence of periodicity.

When the MO test fails to reject its null hypothesis, it indicates that the test signals may be CBNP signals or white Gaussian noise. To further distinguish between the two, we propose a new T^2 test based on a Hotelling's T-squared statistic constructed on the asymptotic multivariate normal distribution of the transformed EnNRC. This test, used after the MO test, can effectively discriminate between white Gaussian noise and correlated signals, because the joint correlation between transformed EnNRC features is fully considered here. It is worth noting that our T^2 test is complementary to the proposed MO test, and is used only when we want to further determine whether nonperiodic signals are CBNP signals.

Based on these two proposed tests, it is straightforward to construct their corresponding control charts, i.e., the MO and T^2 control charts. Moreover, for some practical applications

4

where the signals may not satisfy the null hypothesis of the tests, we propose corresponding EWMA-based control charts as a supplementary tool. These EWMA-based control charts allow the monitoring of state changes (condition monitoring), without requiring the current state to be white Gaussian noises, although they detect deviations from the current state rather than the periodicity itself.

The remainder of this paper is organized as follows. Section 2 provides a review of the spectral control charts and discusses some of their weaknesses. In Section 3, we propose the EnRC feature and study its finite-sample as well as asymptotic properties. In Section 4, we propose the MO and T^2 tests and then construct their corresponding control charts. Numerical examples are presented in Section 5, and a real case study on bearing fault monitoring is conducted in Section 6. Section 7 concludes the paper with a discussion of future research. All proofs are relegated to Supplementary Materials, and the MATLAB code for this work is available on GitHub: https://github.com/Yongxiang-Li/EnRC.

2   Brief Literature Review

A noisy observation $y(t)$ of a process can be modeled as the sum of the source signal $x(t)$ and the white Gaussian noise $\epsilon(t)$:

$$y(t) = x(t) + \epsilon(t), \tag{1}$$

where $\epsilon(t) \sim \mathcal{N}(0, \sigma^2)$. Throughout this work, we assume that the signal $x(t)$ is deterministic, which can be zero (i.e., $y(t)$ is white Gaussian), a correlated series generated from a stationary GP, or a strictly periodic series. Following the settings in Fan et al. (2018), the noisy signal $y(t)$ is observed at the sampling frequency f_s. With the advances in sensing technology, the sampling frequency f_s is often considerably high in practice, and thus it is reasonable to assume that each period has an integer number of points (Li et al., 2023).

This assumption can be easily relaxed by increasing f_s.

Suppose l observed samples are collected at the sampling frequency f_s, and let $\boldsymbol{y} = [y(1), y(2), ..., y(l)]^T$, $\boldsymbol{x} = [x(1), x(2), ..., x(l)]^T$, and $\boldsymbol{\epsilon} = [\epsilon(1), \epsilon(2), ..., \epsilon(l)]^T$. Considering that $\epsilon(t)$ is independent and identically distributed (i.i.d.), we have $\boldsymbol{\epsilon} \sim \mathcal{N}(\boldsymbol{0}, \sigma^2 \boldsymbol{I}_l)$, where $\boldsymbol{I}_l$ is the identity matrix of size $l \times l$. The matrix form of the model in Eq. (1) is $\boldsymbol{y} = \boldsymbol{x} + \boldsymbol{\epsilon}$. If periodicity exists in the noisy signal $\boldsymbol{y}$, $\boldsymbol{x}$ is thought to be periodic with an unknown period. Without loss of generality, we assume the mean of $\boldsymbol{x}$ to be 0.

Periodogram is a commonly used statistic in spectral control charts (Bølviken, 1983; Beneke et al., 1988; Zhao-Guo, 1988; Spurrier and Thombs, 1990; Tatum, 1996) for detecting sinusoidal periodic behaviors in the data. The periodogram of the noisy signals $\boldsymbol{y}$ for a given angular frequency ω is defined as the power spectral density of the signal (McSweeney, 2006b):

$$\mathcal{S}_{\boldsymbol{y}}(\omega) = \frac{1}{l} \left| \sum_{n=1}^{l} y(n) e^{-j\omega n} \right|^2, \tag{2}$$

where j denotes the imaginary unit.

The periodogram is commonly evaluated at Fourier frequencies ($\omega_i = 2\pi i/l$ for $i = 1, 2, \cdots, \lfloor l/2 \rfloor$) by using the discrete Fourier transform, where $\lfloor l/2 \rfloor$ denotes the maximum integer not greater than $l/2$. By utilizing the orthogonality of the discrete Fourier matrix, Fisher (1929) developed a hypothesis test based on the periodogram to identify the existence of periodicity in $\boldsymbol{y}$ under the null hypothesis ($\mathcal{H}_0$) that $\boldsymbol{y}$ is a vector of white Gaussian noise (i.e., $\boldsymbol{y} = \boldsymbol{\epsilon}$). The statistic used in this so-called Fisher's test is

$$\xi = \frac{\max_{i} \mathcal{S}_{\boldsymbol{y}}(\omega_i)}{\frac{1}{h} \sum_{i=1}^{h} \mathcal{S}_{\boldsymbol{y}}(\omega_i)},$$

where $h = \lfloor l/2 \rfloor$ is the number of Fourier frequencies in the periodogram. This statistic would be considerably large if the dominant peak of the periodogram largely exceeds its average (Fuller, 2009). Its closed-form distribution under the null hypothesis is given in

6

Fisher (1929).

Spurrier and Thombs (1990) utilized the trigonometric regression model to construct another spectral control chart, called T chart, for identifying periodicity at non-Fourier frequencies. Its statistic is also based on the periodogram $\mathcal{S}_{\boldsymbol{y}}(\omega)$ in Eq. (2), and the difference lies in the choice of frequency ω in the Fourier basis, which are not necessarily Fourier frequencies. Given that the periodogram ordinates used in the T chart are no longer independent, the close form of the critical value does not exist, and it is often estimated numerically using Monte Carlo (MC) methods.

One common problem with current spectral control charts is that the periodogram used therein is vulnerable to the masking effect of background noise, making these spectral methods less effective for signals with a low signal-to-noise ratio (SNR). As shown in Fig. 1 (a)-(c), the periodogram of the noise $\boldsymbol{\epsilon}$ has a similar amplitude as that of the source signal $\boldsymbol{x}$, making the dominant frequency difficult to identify from the periodogram of the noisy signal $\boldsymbol{y}$. The discrete Fourier transform used in the periodogram is inefficient at suppressing noise, causing the noise spectrum to mask the signal source spectrum. As an illustration, the maximum periodogram of the noise in Fig. 1 (b) equals to that of the noisy signal in Fig. 1 (c), which indicates that Fisher's test may not be able to identify the periodicity under such a scenario. Clearly, the spectral control charts developed on the periodogram do not work effectively under noisy environments (i.e. low-SNR signals) in Fig. 1, because the periodogram is not noise resistant.

Another drawback of spectral control charts is that they are easily misled by the CBNP signals and would mistakenly report them as periodic. This is because they consider the probability conditioned on the null hypothesis rather than the probability conditioned on the hypothesis that periodicity is present. For example, when the source signals $\boldsymbol{x}$ are CBNP, the null hypothesis could be easily rejected by conventional spectral control charts, and $\boldsymbol{x}$ would be reported as periodic (out-of-control events) following the alternative hypothesis. Fig. 2 (b) in Section 4.1 shows a typical periodogram of correlated signals
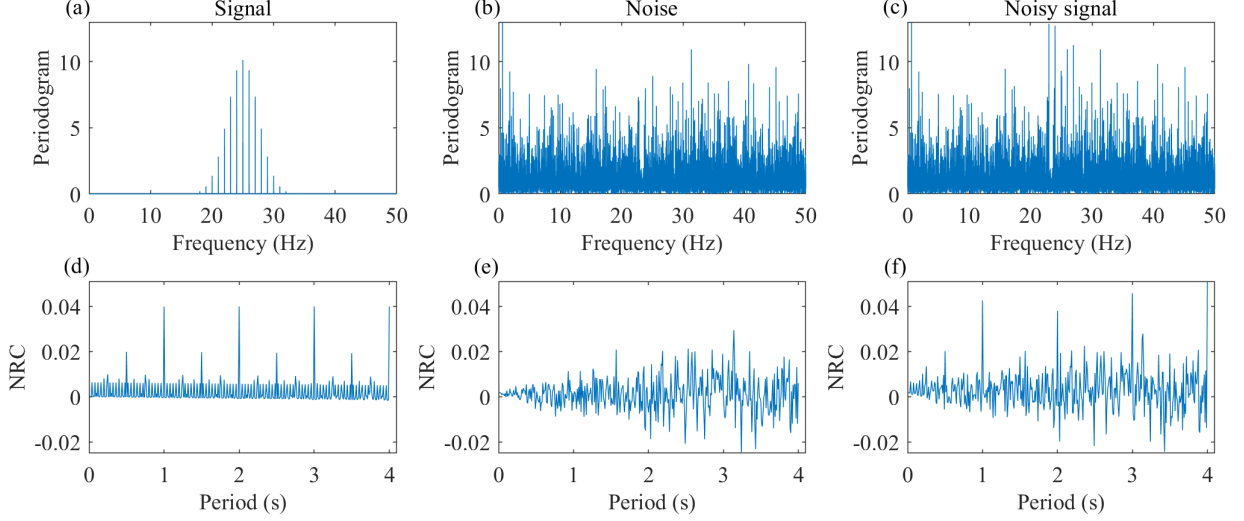
7

Figure 1: Periodogram of (a) the source signal $\boldsymbol{x}$, (b) noise $\boldsymbol{\epsilon}$, and (c) noisy signals $\boldsymbol{y}$; NRC of (d) the source signal $\boldsymbol{x}$, (e) noise $\boldsymbol{\epsilon}$, and (f) noisy signals $\boldsymbol{y}$. The SNR is -18 dB, and the signal length l is 10000.

generated from a stationary GP, which is obviously different from the periodogram of white Gaussian noise.

Fan et al. (2018) proposed a so-called noise resistant correlation (NRC) method, which divides the signal $\boldsymbol{y}$ into $m = \lfloor l/n \rfloor$ segments. The kth segment is denoted as $\boldsymbol{y}_k = [y((k-1)n+1), \cdots, y(kn)]$, where $k = 1, 2, \cdots, m$, and n is the number of samples in each segment. Fan et al. (2018) defined a correlation-based function on these m segments $\{\boldsymbol{y}_1, \boldsymbol{y}_2, \cdots, \boldsymbol{y}_m\}$:

$$\mathcal{Q}_{\boldsymbol{y}}(n) = \frac{\sum\limits_{1 \leq i \neq j \leq m} \boldsymbol{y}_i^T \boldsymbol{y}_j}{m(m-1)n}. \tag{3}$$

Notably, the NRC function $\mathcal{Q}_{\boldsymbol{y}}(n)$ ignores the last $l - mn$ signal points in $\boldsymbol{y}$, which is an incomplete segment.

Different from the periodogram that transforms signals into the frequency domain through spectral analysis, NRC is a time domain method that measures the cross-correlation between signals of different segments. Fan et al. (2018) has demonstrated that the NRC function is more noise resistant than the classic autocorrelation method (Rabiner, 1977).

As an illustration, Fig. 1 (d) shows that NRC has clear peaks at the true period (1 second) and its multiples, indicating that NRC is more robust than the periodogram under the noisy environment.

The NRC feature in Fan et al. (2018) will drop the last incomplete segment of signals when $l > mn$, which may cause considerable information loss, especially when the segment length is long. Additionally, it is unclear how to compute the covariance matrix of the NRC feature in an acceptable time. Furthermore, dropping the last incomplete segment makes the finite-sample properties of NRC hard to analyze and further hinders the analysis of the asymptotic distribution of the NRC features for further statistical hypothesis testing. To the best of our knowledge, there is no current work that can address this problem, which motivates us to propose a new NRC feature that considers all signal points in $\boldsymbol{y}$ and possesses desirable theoretical properties. Finding the asymptotic distribution of features is a common problem for other related signal processing techniques, such as the autogram (Moshrefzadeh and Fasana, 2018). The proposed EnNRC not only extends the NRC features but also studies the finite-sample properties and asymptotic distribution of the features, making it possible to perform statistical hypothesis testing.

3   Enhanced Noise Resistant Correlation

To address the aforementioned issues, we propose a new feature, called the enhanced noise resistant correlation (EnNRC). Compared to NRC, the proposed EnNRC has a lower variance and more attractive finite-sample and asymptotic properties by considering all data points instead of dropping the last $l - mn$ points.

3.1   Formulation of EnNRC

Following the notation in Section 2, the noisy signal $\boldsymbol{y}$ is divided into $m = \lfloor l/n \rfloor$ segments. For the special case when l divides n (i.e., $l \% n = 0$), the proposed EnNRC is the same

as the NRC in Eq. (3). When the signal cannot be exactly divided (i.e., $l \% n \neq 0$), each segment in EnNRC, except for the last one, is further divided into two subsegments. That is, the signal is alternatively divided into $2m + 1$ segments with $o_n = \lceil l/n \rceil$ odd subsegments (where $\lceil l/n \rceil$ denotes the smallest integer no less than l/n) and $e_n = \lfloor l/n \rfloor$ even subsegments. Each odd segment has a length of $n_1 = l - mn$, where $m = \lfloor l/n \rfloor$, and each even segment has a length of $n_2 = n - n_1$. Then, all odd segments are combined to form a new signal

$$
\boldsymbol{y}_o = \begin{bmatrix} \boldsymbol{y}_{1,1}^T, & \boldsymbol{y}_{2,1}^T, & \cdots, & \boldsymbol{y}_{m+1,1}^T \end{bmatrix}^T,
$$

and all even segments are combined to form a new signal

$$
\boldsymbol{y}_e = \begin{bmatrix} \boldsymbol{y}_{1,2}^T, & \boldsymbol{y}_{2,2}^T, & \cdots, & \boldsymbol{y}_{m,2}^T \end{bmatrix}^T.
$$

Two NRC functions are defined on $\boldsymbol{y}_o$ and $\boldsymbol{y}_e$ respectively as follows:

$$
\mathcal{Q}_{\boldsymbol{y}_o}(n_1) = \frac{\sum\limits_{1 \leq i \neq j \leq o_n} \boldsymbol{y}_{i,1}^T \boldsymbol{y}_{j,1}}{o_n (o_n - 1) n_1} \text{ and } \mathcal{Q}_{\boldsymbol{y}_e}(n_2) = \frac{\sum\limits_{1 \leq i \neq j \leq e_n} \boldsymbol{y}_{i,2}^T \boldsymbol{y}_{j,2}}{e_n (e_n - 1) n_2}.
$$

The proposed EnNRC function is defined as a weighted sum of $\mathcal{Q}_{\boldsymbol{y}_o}(n_1)$ and $\mathcal{Q}_{\boldsymbol{y}_e}(n_2)$, i.e., $\mathcal{C}_{\boldsymbol{y}}(n) = \omega_o \mathcal{Q}_{\boldsymbol{y}_o}(n_1) + \omega_e \mathcal{Q}_{\boldsymbol{y}_e}(n_2)$, where $\omega_o = o_n n_1/l$, and $\omega_e = e_n n_2/l$. Without loss of generality, when $l \% n = 0$, we assume $\boldsymbol{y}_{j,1}$ is empty and $\boldsymbol{y}_{j,2} = \boldsymbol{y}_j$, and the inner product of two empty vectors is 0 (i.e., $\boldsymbol{y}_{i,1}^T \boldsymbol{y}_{j,1} = 0$ for all i, j). Then, the EnNRC function $\mathcal{C}_{\boldsymbol{y}}(n)$ can be written as (for any l)

$$
\mathcal{C}_{\boldsymbol{y}}(n) = \frac{\sum\limits_{1 \leq i \neq j \leq o_n} \boldsymbol{y}_{i,1}^T \boldsymbol{y}_{j,1}}{(o_n - 1) l} + \frac{\sum\limits_{1 \leq i \neq j \leq e_n} \boldsymbol{y}_{i,2}^T \boldsymbol{y}_{j,2}}{(e_n - 1) l},
$$

and its matrix form is

$$
\mathcal{C}_{\boldsymbol{y}}(n) = \boldsymbol{y}^T \boldsymbol{C}_n \boldsymbol{y}, \tag{4}
$$

where $\boldsymbol{C}_n = \widetilde{\boldsymbol{C}}_n - \boldsymbol{D}_n$ is an $l \times l$ matrix with

$$\widetilde{\boldsymbol{C}}_n = \begin{bmatrix} \boldsymbol{M}_n & \cdots & \boldsymbol{M}_n & \boldsymbol{W}_n^T \\ \vdots & \ddots & \ddots & \vdots \\ \boldsymbol{M}_n & \cdots & \boldsymbol{M}_n & \boldsymbol{W}_n^T \\ \boldsymbol{W}_n & \cdots & \boldsymbol{W}_n & \boldsymbol{O}_n \end{bmatrix} \text{ and } \boldsymbol{D}_n = \begin{bmatrix} \boldsymbol{M}_n & & & \\ & \ddots & & \\ & & \boldsymbol{M}_n & \\ & & & \boldsymbol{O}_n \end{bmatrix}.$$

Here, $\boldsymbol{M}_n$ is a block diagonal matrix of $\boldsymbol{O}_n$ and $\boldsymbol{E}_n$, and $\boldsymbol{W}_n = \begin{bmatrix} \boldsymbol{O}_n & \boldsymbol{0}_{n_1 \times n_2} \end{bmatrix}$, with

$$\boldsymbol{O}_n = \frac{\boldsymbol{I}_{n_1 \times n_1}}{(o_n - 1)\, l} \text{ and } \boldsymbol{E}_n = \frac{\boldsymbol{I}_{n_2 \times n_2}}{(e_n - 1)\, l}.$$

Similar to $\mathcal{C}_{\boldsymbol{y}}(n)$ in Eq. (4), we define the EnNRC function on the source signal $\boldsymbol{x}$ as $\mathcal{C}_{\boldsymbol{x}}(n) = \boldsymbol{x}^T \boldsymbol{C}_n \boldsymbol{x}$, and that on the noise $\boldsymbol{\epsilon}$ as $\mathcal{C}_{\boldsymbol{\epsilon}}(n) = \boldsymbol{\epsilon}^T \boldsymbol{C}_n \boldsymbol{\epsilon}$. Then, $\mathcal{C}_{\boldsymbol{y}}(n)$ can be further decomposed as

$$\mathcal{C}_{\boldsymbol{y}}(n) = \mathcal{C}_{\boldsymbol{x}}(n) + \mathcal{C}_{\boldsymbol{\epsilon}}(n) + \mathcal{X}_{\boldsymbol{\epsilon}}(n), \tag{5}$$

where $\mathcal{X}_{\boldsymbol{\epsilon}}(n) = 2\boldsymbol{x}^T \boldsymbol{C}_n \boldsymbol{\epsilon}$. It is worth noting that, unlike the EnNRC function, the NRC function cannot be written in a neat form as in Eq. 4, making it difficult to derive appealing finite-sample and asymptotic properties.

3.2 Finite-Sample Properties

The data size is often limited in practice. For accurate inference, we first study the finite-sample properties of the proposed EnNRC in Eq. (4).

Theorem 1. *For any discrete signal $\boldsymbol{x}$ of length l, the inequality*

$$\boldsymbol{x}^T \boldsymbol{C}_n \boldsymbol{x} \leq \|\boldsymbol{x}\|^2 / l$$

holds for any $n < l/2$. The above equality holds if and only if $\boldsymbol{x}$ is periodic and n is a

11

multiple of the period p_0, i.e., $n \in \mathbb{N} = \{p_0, 2p_0, 3p_0, \ldots\}$.

Theorem 1 implies that the expectation of $\mathcal{C}_{\boldsymbol{y}}(n)$ is not greater than the average power $\mathcal{P}_{\boldsymbol{x}}$ of the source signal $\boldsymbol{x}$, i.e.,

$$\mathsf{E}\left[\mathcal{C}_{\boldsymbol{y}}(n)\right] = \mathcal{C}_{\boldsymbol{x}}(n) \leq \mathcal{P}_{\boldsymbol{x}} \tag{6}$$

for any $\boldsymbol{x}$, where $\mathcal{P}_{\boldsymbol{x}} = \left(\boldsymbol{x}^T \boldsymbol{x}\right)/l$. The necessary condition of Theorem 1 implies that the equality holds if and only if the source signals are periodic and the segmentation of signals is correct. Notably, the above inequality is valid even if $\boldsymbol{x}$ is not periodic, which has not been revealed in NRC (Fan et al., 2018).

The inequality in (6) reveals that the proposed EnNRC function behaves similarly to a likelihood function. That is, $\mathsf{E}\left[\mathcal{C}_{\boldsymbol{y}}(n)\right] = \mathcal{P}_{\boldsymbol{x}}$ when $\boldsymbol{x}$ is periodic and $\mathsf{E}\left[\mathcal{C}_{\boldsymbol{y}}(n)\right] < \mathcal{P}_{\boldsymbol{x}}$ when $\boldsymbol{x}$ is not periodic. Additionally, we have $\mathsf{E}\left[\mathcal{C}_{\boldsymbol{y}}(n)\right] = 0$ when the signals $\boldsymbol{y}$ are white Gaussian noise. Thus, the proposed features have a sound potential for effectively detecting periodicity.

It is worth remarking that $\boldsymbol{C}_n \boldsymbol{x} = \boldsymbol{x}/l$ when $\boldsymbol{x}$ is periodic, and this equality holds if and only if $\boldsymbol{x}$ is periodic with period p_0 and $n \in \mathbb{N}$. This equality means that $1/l$ is one eigenvalue of $\boldsymbol{C}_n$. The maximum eigenvalue of $\boldsymbol{C}_n$ is $1/l$ because $\lambda_{max} = \max_{\|\boldsymbol{x}\|=1} \boldsymbol{x}^T \boldsymbol{C}_n \boldsymbol{x} = 1$ according to Theorem 1. Likewise, the smallest eigenvalue of $\boldsymbol{C}_n$ is greater than $-1/l$.

The covariance matrix of $\mathcal{C}_{\boldsymbol{\epsilon}}^{(1:p)} = \left[\mathcal{C}_{\boldsymbol{\epsilon}}(1), \mathcal{C}_{\boldsymbol{\epsilon}}(2), \cdots, \mathcal{C}_{\boldsymbol{\epsilon}}(p)\right]^T$ is denoted by $2\sigma^4 \boldsymbol{\Sigma}_l$, where p is the number of inspection periods, and

$$\boldsymbol{\Sigma}_l = \begin{bmatrix} \mathrm{Tr}\left(\boldsymbol{C}_1 \boldsymbol{C}_1\right) & \cdots & \mathrm{Tr}\left(\boldsymbol{C}_1 \boldsymbol{C}_p\right) \\ \vdots & \ddots & \vdots \\ \mathrm{Tr}\left(\boldsymbol{C}_p \boldsymbol{C}_1\right) & \cdots & \mathrm{Tr}\left(\boldsymbol{C}_p \boldsymbol{C}_p\right) \end{bmatrix}. \tag{7}$$

A fast computing formula for $\mathrm{Tr}\left(\boldsymbol{C}_i \boldsymbol{C}_j\right)$ is provided in Eq. (21), which will be discussed in Section 4.3.

Theorem 2. *The matrix $\boldsymbol{\Sigma}_l$ is positive definite if $l > p + 1$.*

To test the existence of periodicity, the finite-sample covariance matrix $2\sigma^4\boldsymbol{\Sigma}_l$ is needed for constructing the MO statistic in practice. Using the finite-sample (rather than asymptotic) covariance matrix can increase the accuracy of the test, especially when the signal length l is short, because the asymptotic covariance matrix is only valid when the signal length l is infinite.

3.3 Iterative Hypothesis Testing based on Dynamic Significance Levels

To begin with, we show that the value of EnNRC will converge to its expectation in probability, which suggests that using an appropriate statistic designed on EnNRC can effectively detect the periodicity in the noisy signals $\boldsymbol{y}$.

Theorem 3. *As the signal length goes to infinity, the EnNRC function $\mathcal{C}_{\boldsymbol{y}}(n)$ converges to its expectation $\mathcal{C}_{\boldsymbol{x}}(n)$ in probability, i.e.,*

$$\mathcal{C}_{\boldsymbol{y}}(n) - \mathcal{C}_{\boldsymbol{x}}(n) \xrightarrow{p} 0, \ \ as \ l \to \infty. \tag{8}$$

Next, we study the joint distribution of the EnNRC features, as $\{\mathcal{C}_{\boldsymbol{y}}(n)\}$ $(n = 1, 2, \cdots)$ are not independent. Considering that the test statistics are commonly designed under the null hypothesis (i.e., $\boldsymbol{y} = \boldsymbol{\epsilon}$) in literature (Fisher, 1929), we also focus on the joint distribution of $\{\mathcal{C}_{\boldsymbol{y}}(n)\}$ under the null hypothesis, i.e., the joint distribution of $\{\mathcal{C}_{\boldsymbol{\epsilon}}(n)\}$.

Lemma 1. *The matrix $l^2\boldsymbol{\Sigma}_l$ converges to the greatest common divisor (GCD) matrix $\boldsymbol{\Sigma}$*

on the set $\{1, 2, \cdots, p\}$ as l goes to infinity, i.e.,

$$\lim_{l \to \infty} l^2 \boldsymbol{\Sigma}_l = \boldsymbol{\Sigma} = \begin{bmatrix} (1,1) & \cdots & (1,p) \\ \vdots & \ddots & \vdots \\ (p,1) & \cdots & (p,p) \end{bmatrix}, \tag{9}$$

where (i,j) denotes the GCD of i and j.

Lemma 1 shows that $\lim_{l \to \infty} l^2 \mathrm{Tr}\left(\boldsymbol{C}_i \boldsymbol{C}_j\right) = (i,j)$. It reveals that the covariance matrix of $l \mathcal{C}_{\boldsymbol{\epsilon}}^{(1:p)}$ (which is $2\sigma^4 l^2 \boldsymbol{\Sigma}_l$) converges to $2\sigma^4 \boldsymbol{\Sigma}$ as the signal length l goes to infinity, where $\boldsymbol{\Sigma}$ is the GCD matrix. Notably, Beslin and Ligh (1989) showed that every GCD matrix is positive definite and thus nonsingular.

Lemma 2. *The standardized value of $\mathcal{C}_{\boldsymbol{\epsilon}}(n)$ will converge in distribution to a standard normal random variable as the signal length l goes to infinity, i.e.,*

$$\frac{\mathcal{C}_{\boldsymbol{\epsilon}}(n)}{\sqrt{\mathsf{V}\left(\mathcal{C}_{\boldsymbol{\epsilon}}(n)\right)}} \xrightarrow{d} \mathcal{N}(0,1), \ \ as \ l \to \infty. \tag{10}$$

Lemma 3. *The standardized value of $\mathcal{C}_{\boldsymbol{\epsilon}}(p) - \sum_{n=1}^{p-1} \alpha_n \mathcal{C}_{\boldsymbol{\epsilon}}(n)$ will converge in distribution to a standard normal random variable as the signal length l goes to infinity, i.e.,*

$$\frac{\mathcal{C}_{\boldsymbol{\epsilon}}(p) - \sum_{n=1}^{p-1} \alpha_n \mathcal{C}_{\boldsymbol{\epsilon}}(n)}{\sqrt{\mathsf{V}\left(\mathcal{C}_{\boldsymbol{\epsilon}}(p) - \sum_{n=1}^{p-1} \alpha_n \mathcal{C}_{\boldsymbol{\epsilon}}(n)\right)}} \xrightarrow{d} \mathcal{N}(0,1), \ \ as \ l \to \infty. \tag{11}$$

Lemma 2 provides the asymptotic normal distribution of $\mathcal{C}_{\boldsymbol{\epsilon}}(n)$, and Lemma 3 demonstrates the asymptotic normal distribution of $\mathcal{C}_{\boldsymbol{\epsilon}}(p) - \sum_{n=1}^{p-1} \alpha_n \mathcal{C}_{\boldsymbol{\epsilon}}(n)$ for any α_n. Then, through the Cramer-Wold theorem (Cramér and Wold, 1936), we can prove the asymptotic multivariate normal distribution of $\mathcal{C}_{\boldsymbol{\epsilon}}^{(1:p)}$, as shown in the following theorem.

Theorem 4. *The vector of EnNRCs $\mathcal{C}_{\boldsymbol{\epsilon}}^{(1:p)}$ asymptotically follows a multivariate normal distribution as $l \to \infty$, i.e.,*

$$l\mathcal{C}_{\boldsymbol{\epsilon}}^{(1:p)} \xrightarrow{d} \mathcal{N}\left(\mathbf{0}, 2\sigma^4 \boldsymbol{\Sigma}\right). \tag{12}$$

Theorem 4 shows that the EnNRCs $\mathcal{C}_{\boldsymbol{\epsilon}}^{(1:p)}$ converge in distribution to a multivariate normal distribution. Thus, the EnNRCs $\{\mathcal{C}_{\boldsymbol{y}}(n)\}$ asymptotically follow a multivariate normal distribution under the null hypothesis, and its asymptotic covariance matrix is $2\sigma^4 \boldsymbol{\Sigma}$. Notably, such theoretical properties of EnNRC have not yet been found in NRC (Fan et al., 2018).

4 Robust Periodicity Detection and Monitoring

On the basis of the theoretical properties of the proposed EnNRC features, we construct two test statistics, called the MO test and the T^2 test. The MO test is designed to detect periodicity, while the T^2 test complements to the correlation detection if we want to discriminate between CBNP signals and white Gaussian noise. Additionally, a fast computing formula of the covariance matrix is developed to speed up the proposed tests.

4.1 Testing Periodic versus Nonperiodic Signals

In this part, we introduce a hypothesis test that aims to distinguish between white Gaussian noise and periodic signals. The hypothesis is defined as follows:

$$\begin{cases} \mathcal{H}_0: & \boldsymbol{y} \text{ is a vector of white Gaussian noise,} \\ \mathcal{H}_1: & \boldsymbol{y} \text{ is a vector of contaminated periodic signals.} \end{cases} \tag{13}$$

Under the null hypothesis $\mathcal{H}_0$, the observed signals $\boldsymbol{y}$ are white Gaussian noise with source signals $\boldsymbol{x}$ vanishing to 0. Under the alternative hypothesis $\mathcal{H}_1$, the observed signals $\boldsymbol{y}$ are periodic signals contaminated with white Gaussian noise.

As previously discussed, not all correlated signals exhibit periodicity. For example, some correlated time series such as GPs are nonperiodic (i.e., CBNP), but they are often mistakenly reported as periodic by conventional spectral control charts. To address this problem, we propose a new test that can effectively distinguish between periodic and nonperiodic signals (including white Gaussian noises and CBNP signals).

According to the asymptotic multivariate normal distribution in Eq. (12), a test statistic can be constructed on the EnNRC features $\mathcal{C}_{\boldsymbol{y}} = [\mathcal{C}_{\boldsymbol{y}}(p_1), \cdots, \mathcal{C}_{\boldsymbol{y}}(p_q)]^T$, where $p_1, \cdots, p_q$ are the inspection periods. We denote the covariance matrix of $\mathcal{C}_{\boldsymbol{\epsilon}}$ as $2\sigma^4 \boldsymbol{\Xi}_l$, which is the corresponding sub-matrix of $2\sigma^4 \boldsymbol{\Sigma}_l$. Notably, the matrix $\boldsymbol{\Xi}_l$ is strictly positive definite according to Lemma 2.

The correlated EnNRC features $\mathcal{C}_{\boldsymbol{y}}$ are transformed into another space:

$$\mathcal{O}_{\boldsymbol{y}} = \boldsymbol{L}^{-1} \mathcal{C}_{\boldsymbol{y}}, \tag{14}$$

where $\boldsymbol{L}$ is a lower triangular matrix yielded by the Cholesky decomposition of $\boldsymbol{\Xi}_l$. Under the null hypothesis $\mathcal{H}_0$, the covariance matrix of $\mathcal{C}_{\boldsymbol{y}}$ is $2\sigma^4 \boldsymbol{\Xi}_l$, and thus the transformation in Eq. (14) is orthogonal. This transformation converts the correlated noise resistant features $\mathcal{C}_{\boldsymbol{y}}$ into the white Gaussian features $\mathcal{O}_{\boldsymbol{y}}$ under $\mathcal{H}_0$. Fig. 2 (d) further verifies that the transformed features $\mathcal{O}_{\boldsymbol{y}}$ are i.i.d. under $\mathcal{H}_0$, which is consistent with their theoretical distribution.

To improve the numerical stability of computing $\mathcal{O}_{\boldsymbol{y}}$, the inspection periods $p_1, \cdots, p_q$ should be given in decreasing order, i.e., $p_1 > p_2 > \cdots > p_q$. In most applications, we recommend setting $p_1, \cdots, p_q$ as q consecutive decreasing integers with $p_1 = q + 1$. By default, it is recommended that $q = \lfloor l/10 \rfloor$, i.e., 1/10th of the signal length, which generally provides excellent performance as shown in our numerical examples. To ensure the convergence of the asymptotic distribution in Theorem 4, this proportion should not be too high. For example, $q = \lfloor l/2 \rfloor$ or $q = \lfloor l/3 \rfloor$ is not appropriate because the number of signal

segments is not sufficient for the asymptotic distribution to converge well. Considering the computation time of calculating $\mathbf{\Sigma}_l$, a smaller proportion (e.g., $\lfloor l/15 \rfloor$ or $\lfloor l/20 \rfloor$) may be used when the signal length is considerably large.

We propose the maximum order (MO) statistic of normalized $\mathcal{O}_{\boldsymbol{y}}(p_i)$ (which is the ith element of $\mathcal{O}_{\boldsymbol{y}} = [\mathcal{O}_{\boldsymbol{y}}(p_1), \cdots, \mathcal{O}_{\boldsymbol{y}}(p_q)]^T$) to recognize the periodicity from the correlated signals, i.e.,

$$M = \max_{i \in \{1,2,\cdots,q\}} \frac{\mathcal{O}_{\boldsymbol{y}}(p_i) - \mu_{\mathcal{O}_{\boldsymbol{y}}}}{\sigma_{\mathcal{O}_{\boldsymbol{y}}}}, \tag{15}$$

where $\mu_{\mathcal{O}_{\boldsymbol{y}}}$ and $\sigma^2_{\mathcal{O}_{\boldsymbol{y}}}$ are the sample mean and variance of $\mathcal{O}_{\boldsymbol{y}}(p_i)$. We use M in Eq. (15) as the statistic for the hypothesis testing in Eq. (13). The MO statistic M is the maximum value of q i.i.d. standard normal variables under $\mathcal{H}_0$, and its closed-form cumulative distribution is

$$P(M \leq x) = \{\Phi(x)\}^q, \tag{16}$$

where $\Phi(x)$ is the cumulative distribution function of the standard normal random variable. The control chart that employs the MO test to monitor the existence of periodicity in a process is called the MO control chart. Given a predetermined significance level α, the control limit M_α for the MO control chart can be identified.

When the test signals are correlated (not necessarily periodic), the transformed EnNRC features $\mathcal{O}_{\boldsymbol{y}}$ are not independent, because the correlation in $\boldsymbol{y}$ will be transmitted to $\mathcal{O}_{\boldsymbol{y}}$. For example, $\mathcal{O}_{\boldsymbol{y}}$ in Fig. 2 (e) and (f) are much smoother than those in Fig. 2 (d). This phenomenon suggests that ignoring the correlation between the transformed EnNRC features $\mathcal{O}_{\boldsymbol{y}}$ could reduce the risk of reporting the CBNP signals as periodic.

Recall that the EnNRCs $\mathcal{C}_{\boldsymbol{y}}$ have clear peaks at the true period and its multiple if the signals are periodic. These peaks will be inherited by $\mathcal{O}_{\boldsymbol{y}}$. As an illustration, Fig. 2 (f) shows that the orthogonal features have clear peaks at the true period and its multiples when the test signals $\boldsymbol{y}$ are periodic; by contrast, in Fig. 2 (e), no clear peak is observed. This finding demonstrates that the proposed MO test could effectively detect the periodicity
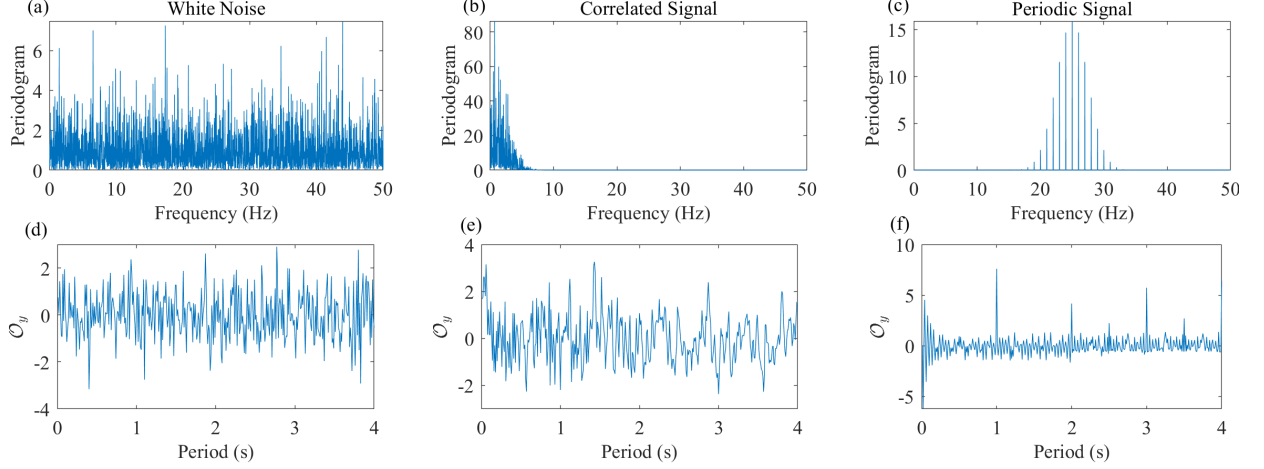
17

Figure 2: Periodogram and transformed EnNRC features: (a) periodogram of white Gaussian noise, (b) periodogram of correlated signals, (c) periodogram of periodic signals, (d) transformed EnNRC of white Gaussian noise, (e) transformed EnNRC of correlated signals, and (f) transformed EnNRC of periodic signals.

in the signal.

The MO test can further distinguish the periodicity from the correlation by considering the highest peak of the transformed EnNRC features. Compared with that in Fig. 2 (e), the maximum value of the periodogram in Fig. 2 (b) is more distinguishable. Hence, the MO test using the maximum value as the test statistic can achieve a lower false alarm rate than conventional spectral methods because taking the maximum value can reduce the impact caused by the correlation within $\mathcal{O}_{\boldsymbol{y}}$. If the null hypothesis is rejected in the MO test, we can conclude that the testing signals are periodic; otherwise nonperiodic. Notably, the nonperiodic signals can be either white Gaussian noise or correlated signals. Thus, new technique is needed if we want to further distinguish between white Gaussian noise and correlated signals.

The control chart that simply employs the MO statistic to monitor the existence of periodicity in a process is called the MO control chart. However, the signals in practical applications may not always strictly satisfy the null hypothesis of the MO test. In such cases, an EWMA-based control chart can be utilized for condition monitoring because it is applicable even if the null hypothesis does not hold. Following the condition monitoring

method proposed in Fan et al. (2022, 2024), an MO-EWMA control chart is constructed based on the MO statistic. The EWMA statistic Z_i at the ith epoch is calculated using the following recursive formula (Montgomery, 2019):

$$Z_i = \lambda M_i + (1 - \lambda)Z_{i-1}, \tag{17}$$

where M_i represents the MO statistic of the ith epoch, λ is the smoothing parameter typically in the range of $0.05 \leq \lambda \leq 0.25$, and Z_0 is often initialized to the process mean μ_0 (the sample mean of the MO statistics in practice). This version serves as a valuable supplement to the original MO control chart, allowing for state change monitoring (condition monitoring) without requiring the current state to be white Gaussian noises. However, unlike the MO control chart, which can detect the existence of periodicity, the MO-EWMA control chart can only detect changes (not necessarily the appearance of periodicity) that deviate from the current state.

4.2 Testing White Gaussian Noise versus Correlated Signals

Considering that the primary objective of the proposed MO test is to detect periodicity in signals, we can accurately determine the presence of periodicity when the null hypothesis is rejected. If we wish to further test the presence of correlation when the null hypothesis is not rejected, the T^2 test can be employed as a supplementary method to discriminate between white Gaussian noises and CBNP signals.

To distinguish between the two types of the aforementioned nonperiodic signals, we consider the following hypothesis test:

$$\begin{cases} \mathcal{H}_0 : & \boldsymbol{y} \text{ is a vector of white Gaussian noise,} \\ \mathcal{H}_2 : & \boldsymbol{y} \text{ is a vector of correlated signals.} \end{cases} \tag{18}$$

Notably, $\boldsymbol{y}$ can be either periodic or nonperiodic under $\mathcal{H}_2$. According to the asymptotic

multivariate normal distribution of EnNRC in Theorem 4, we propose a statistic in the following theorem to test the hypothesis in Eq. (18).

Theorem 5. *The statistic*

$$\mathrm{T}^2 = \frac{1}{2\sigma^4}\mathcal{C}_{\boldsymbol{y}}^T \boldsymbol{\Xi}_l^{-1}\mathcal{C}_{\boldsymbol{y}}$$

asymptotically follows a chi-square distribution with q degrees of freedom under the null hypothesis $\mathcal{H}_0$, i.e.,

$$\mathrm{T}^2 \xrightarrow{d} \chi^2(q). \tag{19}$$

Given that the signals $y(t)$ are white Gaussian noises under the null hypothesis $\mathcal{H}_0$ and will be standardized in advance, we can assume $\sigma^2 = 1$ without loss of generality. Then, the developed T^2 statistic in Theorem 5 can be written as

$$\mathrm{T}^2 = \mathcal{O}_{\boldsymbol{y}}^T \mathcal{O}_{\boldsymbol{y}} = \frac{1}{2}\mathcal{C}_{\boldsymbol{y}}^T \boldsymbol{\Xi}_l^{-1}\mathcal{C}_{\boldsymbol{y}}. \tag{20}$$

We refer to the corresponding test and control chart as the T^2 test and the T^2 control chart, respectively. The critical value χ_α^2, i.e., the control limit of the T^2 control chart, is the upper $100(1-\alpha)$ percentage point of the chi-squared distribution with q degrees of freedom. Similar to the MO-EWMA control chart, as a supplementary approach, we propose a T^2-EWMA control chart based on the T^2 statistic, which is computed as follows (Montgomery, 2019):

$$Z_i = \lambda \mathrm{T}_i^2 + (1-\lambda)Z_{i-1},$$

where T_i^2 represents the T^2 statistic of the epoch i, and Z_i is typically initialized to the sample mean of the T^2 statistics.

The transformed EnNRC features $\mathcal{O}_{\boldsymbol{y}}$ constructed on the correlated signals $\boldsymbol{y}$ will be smoother than those constructed on white Gaussian noise because they inherit the correlation within the signals $\boldsymbol{y}$. As an illustration, $\mathcal{O}_{\boldsymbol{y}}$ in Fig. 2 (e) is clearly smoother than that

in Fig. 2 (d). Because the T^2 test considers the correlation in the transformed EnRC features, it tends to reject the null hypothesis $\mathcal{H}_0$ when the signals are correlated.

Unlike the MO test, the T^2 test itself cannot effectively discriminate whether the test signals $\boldsymbol{y}$ are periodic, because it may exceed the critical value when the signals are CBNP. Fisher's test has similar problems in detecting correlated signals because the correlation within the testing signals can increase the maximum value of the periodogram. It worth noting that using the MO test alone is enough for detecting periodicity from correlation. If we want to further determine whether the testing signals are CNBP, we advocate using the T^2 test only after the MO test reports the signals as nonperiodic.

The simulation studies in Section 5 nevertheless verify that the T^2 test is effective in distinguishing white Gaussian noise from correlated signals. Notably, when applied alone, the T^2 test is still more effective than Fisher's test for detecting periodicity, even though it is designed for detecting correlations; see Section 5 for some examples.

4.3 Fast Computation of Test Statistics

Using the finite-sample covariance matrix (instead of its asymptotic form) to construct the test statistics will increase the accuracy of the proposed MO and T^2 tests, especially when the signal length l is short. However, computing the covariance matrix $\boldsymbol{\Sigma}_l$ in a straightforward way requires a time complexity of $\mathcal{O}\left(p^2 l^2\right)$ which can be considerably slow for large l, where p is the number of inspection periods. Here, we propose a fast formula for computing $\boldsymbol{\Sigma}_l$ with a time complexity less than $\mathcal{O}\left(p^2 l\right)$.

Let $[i, j]$ denote the least common multiple (LCM) of i and j. We first define

$$
\widetilde{\boldsymbol{C}}_i = \begin{bmatrix} \boldsymbol{M}^i_{[i,j]} & \cdots & \boldsymbol{M}^i_{[i,j]} & \left(\boldsymbol{W}^i_{[i,j]}\right)^T \\ \vdots & \ddots & \ddots & \vdots \\ \boldsymbol{M}^i_{[i,j]} & \cdots & \boldsymbol{M}^i_{[i,j]} & \left(\boldsymbol{W}^i_{[i,j]}\right)^T \\ \boldsymbol{W}^i_{[i,j]} & \cdots & \boldsymbol{W}^i_{[i,j]} & \boldsymbol{O}^i_{[i,j]} \end{bmatrix} \text{ and } \boldsymbol{M}^i_{[i,j]} = \underbrace{\begin{bmatrix} \boldsymbol{M}_i & \cdots & \boldsymbol{M}_i \\ \vdots & \ddots & \vdots \\ \boldsymbol{M}_i & \cdots & \boldsymbol{M}_i \end{bmatrix}}_{\text{repeat } [i,j]/i \text{ times}},
$$

where $\boldsymbol{W}^i_{[i,j]}$ is the corresponding sub-matrix of $\boldsymbol{M}^i_{[i,j]}$, and so is $\boldsymbol{O}^i_{[i,j]}$. Thus,

$$
\mathrm{Tr}\left(\boldsymbol{C}_i \boldsymbol{C}_j\right) = e_{[i,j]}\left(e_{[i,j]} - 1\right) \mathrm{Tr}\left(\boldsymbol{M}^i_{[i,j]} \boldsymbol{M}^j_{[j,i]}\right) + 2e_{[i,j]}\mathrm{Tr}\left(\left(\boldsymbol{W}^i_{[i,j]}\right)^T \boldsymbol{W}^j_{[j,i]}\right),
$$

where $e_{[i,j]}$ is defined in a similar way to the definition of e_n in Section 3.1. We have

$$
\mathrm{Tr}\left(\boldsymbol{M}^i_{[i,j]} \boldsymbol{M}^j_{[j,i]}\right) = \left(\boldsymbol{d}^i_{[i,j]}\right)^T \boldsymbol{d}^j_{[j,i]} \text{ and } \mathrm{Tr}\left(\left(\boldsymbol{W}^i_{[i,j]}\right)^T \boldsymbol{W}^j_{[j,i]}\right) = \left(\boldsymbol{o}^i_{[i,j]}\right)^T \boldsymbol{o}^j_{[j,i]},
$$

where the vector $\boldsymbol{d}^i_{[i,j]}$ is the diagonal of $\boldsymbol{M}^i_{[i,j]}$, and the vector $\boldsymbol{o}^i_{[i,j]}$ is the diagonal of $\boldsymbol{O}^i_{[i,j]}$. Then, a fast formula for computing $\mathrm{Tr}\left(\boldsymbol{C}_i \boldsymbol{C}_j\right)$ can be obtained as

$$
\mathrm{Tr}\left(\boldsymbol{C}_i \boldsymbol{C}_j\right) = e_{[i,j]}\left(e_{[i,j]} - 1\right)\left(\boldsymbol{d}^i_{[i,j]}\right)^T \boldsymbol{d}^j_{[j,i]} + 2e_{[i,j]}\left(\boldsymbol{o}^i_{[i,j]}\right)^T \boldsymbol{o}^j_{[j,i]}. \tag{21}
$$

Specifically, we have

$$
\begin{cases} \mathrm{Tr}\left(\boldsymbol{C}_i \boldsymbol{C}_j\right) = 0 & \text{if } [i, j] > l \\ \mathrm{Tr}\left(\boldsymbol{C}_n \boldsymbol{C}_n\right) = \frac{1}{l^2}\left(\frac{o_n n_1}{o_n - 1} + \frac{e_n n_2}{e_n - 1}\right) & \text{if } n < l \end{cases}. \tag{22}
$$

Eqs. (21) and (22) provide a fast approach for computing $\boldsymbol{\Sigma}_l$. Given that evaluating Eq. (21) requires no more than $\mathcal{O}\left([i, j]\right)$, the time complexity for computing $\boldsymbol{\Sigma}_l$ is less than $\mathcal{O}\left(p^2 l\right)$. Notably, it is not required to evaluate Eq. (21) when $[i, j] > l$. It is worth noting
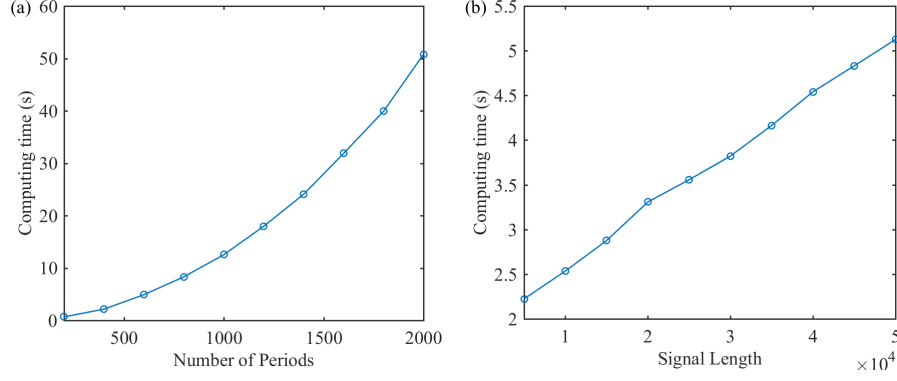
22

Figure 3: Average computing time of the covariance matrix $\boldsymbol{\Sigma}_l$ versus (a) the number of inspection periods p by fixing $l = 5000$ or (b) the signal length l by fixing $p = 400$.

that directly computing the covariance matrix $\boldsymbol{\Sigma}_l$ according to its definition in Eq. (7) is extremely time-consuming. In contrast, when all the points are taken into account, $\boldsymbol{\Sigma}_l$ has a neat structure and an appealing formula, as shown in Eq. (21). We find that this fast computing formula not applicable in NRC because the last incomplete segment is dropped.

Here, we conduct an experiment with 10 independent trials and compare the average computing time of $\boldsymbol{\Sigma}_l$ using Eq. (21). In Fig. 3, the computing time used by our approach increases quadratically with p and linearly with l, which is consistent with the theoretical finding. Specifically, as shown in Fig. 3 (b), our approach requires less than 2.5 seconds for the case of $p = 400$ and $l = 5000$, whereas a direct computation of $\boldsymbol{\Sigma}_l$ requires more than 10 hours for the same case. Additionally, when the signal length increases to $l = 50000$, our approach would only require less than 5.5 seconds. Notably, evaluating the MO and T^2 statistics only requires computing $\boldsymbol{\Sigma}_l$ once, because the signal length l is often fixed in real applications. Moreover, $\boldsymbol{\Sigma}_l$ can be computed and stored before signals are collected. Thus, the proposed test statistics can be used for both online and offline monitoring of periodicity.

23

5 Simulation Study

In this section, simulations are conducted to study the performance of the proposed MO and T^2 tests, as well as their control charts, on periodic and CBNP signals. Here, we aim to compare the performance of the proposed method with some conventional spectral methods, including Fisher's test (Beneke et al., 1988) and T Test (Spurrier and Thombs, 1990), for detecting periodicity.

5.1 Hypothesis Testing on Periodic Signals

In this part, we consider the source signals sampled from the following formula as in Fan et al. (2018):

$$x\left(t\right) = \sum_{k=0}^{\lfloor l/p_0 \rfloor} e^{\frac{-\zeta 2\pi \frac{f_n}{f_s}(t-kp_0)^2}{\sqrt{1-\zeta^2}}} \cos 2\pi \frac{f_n}{f_s}\left(t - kp_0\right), \tag{23}$$

where $\zeta = 0.002$ is the damping ratio, $f_n = 40$ Hz is the natural frequency, $p_0 = 100$ is the number of sampling points in a period, and $f_s = 100$ Hz is the sampling frequency. The period of the signals is 1 second as $p_0 = 100$, indicating that the periodic pattern repeats itself once every second. The amplitude of the signals will be modulated by the natural frequency, complicating the period detection of the signals. We add white Gaussian noise to the source signal $x\left(t\right)$ to generate the synthetic signal $y\left(t\right)$. In this study, SNR is defined as the ratio of the power of the source signal to the power of noise.

Throughout this simulation section, unless otherwise noted, we compute the test statistics of the proposed tests at the inspection period $p_i = \lfloor l/10 \rfloor - i + 2$ for $i = 1, 2, \cdots, \lfloor l/10 \rfloor$, i.e., $\mathcal{C}_{\boldsymbol{y}} = [\mathcal{C}_{\boldsymbol{y}}(\lfloor l/10 \rfloor + 1), \mathcal{C}_{\boldsymbol{y}}(\lfloor l/10 \rfloor), \cdots, \mathcal{C}_{\boldsymbol{y}}(2)]^T$. a significance level of $\alpha = 0.01$ is applied to all tests, and 5000 independent trials are simulated to estimate the statistical power of each method, where the statistical power is the proportion of iterations that correctly reject the null hypothesis $\mathcal{H}_0$. The T test uses the frequencies $\omega_i = \pi i/l$ for $i = 1, 2, \cdots, l$, which are twice as many as those in Fisher's test. The critical value used in the T test is
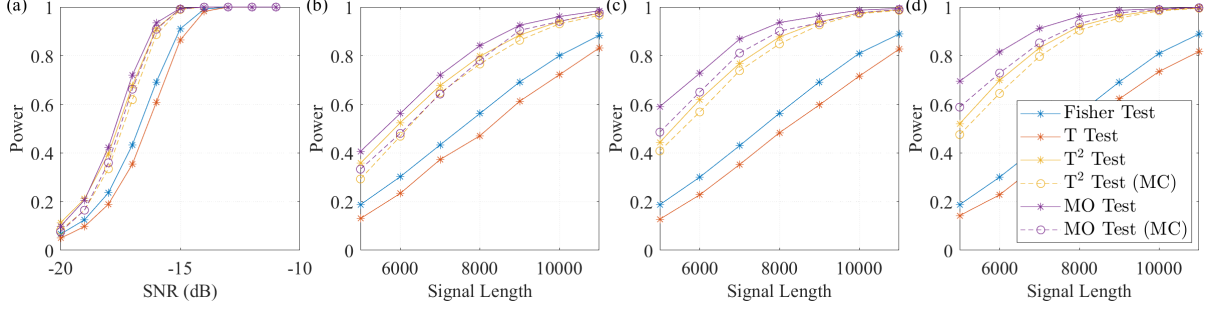
Figure 4: Power of the tests for periodic signals with different SNR levels and signal lengths, where $q = \lfloor l/10 \rfloor$ in (a)-(b), $q = \lfloor l/15 \rfloor$ in (c), and $q = \lfloor l/20 \rfloor$ in (d).

obtained via 10000 MC simulations. The MC versions of the proposed MO and T^2 tests are also shown to study the difference between the empirical and asymptotic distributions of the proposed statistics. Similar to that of the T test, their critical values are obtained via 10000 MC simulations.

Several simulations are conducted under the above settings. In Fig. 4 (a), we consider the cases with l fixed at 7000 and varying SNRs ranging from -20 dB to -11 dB. In Fig. 4 (b), we consider a fixed SNR at -17 dB and varying signal lengths l ranging from 5000 to 11000. To study the impact of q on the performance of the proposed methods, we change q to $\lfloor l/15 \rfloor$ and $\lfloor l/20 \rfloor$, and the corresponding results are shown in Fig. 4 (c) and (d).

In Fig. 4, it is seen that the powers of Fisher's test and the T test are much lower than those of the proposed tests in all cases. In Fig. 4 (a), the powers of the proposed tests converge to 1 when SNR is higher than -15 dB, whereas the powers of Fisher's test and the T test reach 1 when the SNR is higher than -13 dB. Moreover, as shown in Fig. 4 (b), for periodic signals with a relatively low SNR (e.g., -17 dB), both Fisher's test and the T test cannot effectively detect the periodicity (i.e., with power clearly less than 1), even when the signals are very long (e.g., $l = 11000$). Fig. 4 shows that the MO test, among the four tests, consistently gives the best performance in all cases. The MO test can not only effectively detect the periodicity in lower-SNR cases but also detect the periodicity earlier (i.e., requiring shorter signals) than conventional spectral methods. Fig. 4 (b)-(d)

25

demonstrate that our methods are not particularly sensitive to the choice of q.

Additionally, Fig. 4 shows that the MO test gives very close results to its MC version, and so is the T^2 test. This proximity indicates that the critical value computed from the asymptotic distribution is considerably accurate. Furthermore, Fig. 4 (b) shows that the statistical power of the proposed MO and T^2 tests converge to their MC versions as the signal length increases, indicating that the empirical distributions of the test statistics converge to the proposed theoretical distributions in Eqs. (16) and (19), respectively. Thus, we recommend applying the proposed MO and T^2 tests rather than their MC versions in practice, as they are much faster.

Notably, the T test performs worst in this example, even though it employs more frequencies than Fisher's test. A key reason is that its test statistic is calculated via trigonometric regression using a larger frequency basis whose denominator is the sample variance that will be significantly affected by the noise level. As a result, the critical value in the T test, which is computed by MC simulations, is higher than that in Fisher's test. Given that the frequency ordinate of the maximum periodogram is located at the Fourier frequency in this example, more non-Fourier frequencies in the T test will not increase the value of the statistic, leading to a lower power compared with that in Fisher's test. Yet, when the same periodogram ordinates are chosen at the Fourier frequencies in some additional simulations, these two tests may perform similarly. Moreover, when the true frequency of the periodic signals is not at the Fourier frequencies, the T test could outperform Fisher's test, as demonstrated in Spurrier and Thombs (1990) and Tatum (1996).

5.2   Hypothesis Testing on Correlated Signals

Although conventional spectral tests can reject the null hypothesis for periodic signals, they may mistakenly report some CBNP signals as periodic. In this part, we will further evaluate the performance of our proposed tests on the CBNP signals which are simulated
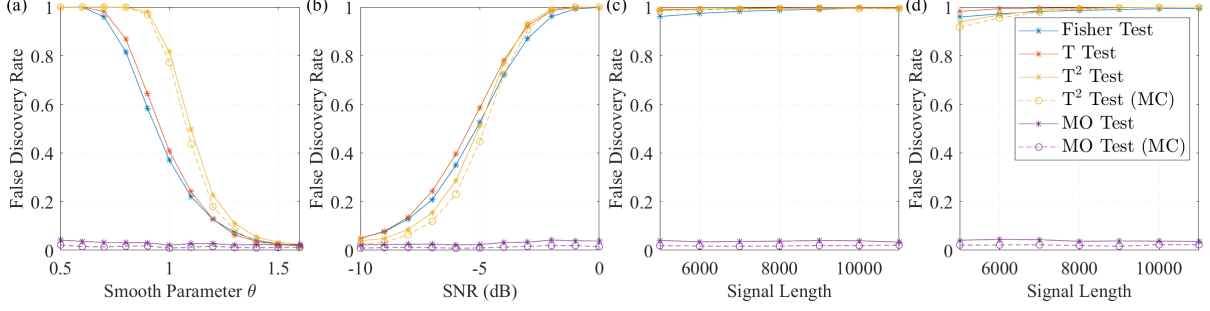
Figure 5: FDRs of the tests on stationary GP signals with different (a) smoothness parameters, (b) SNRs, and (c)-(d) signal lengths, where $q = \lfloor l/10 \rfloor$ in (a)-(c) and $q = \lfloor l/20 \rfloor$ in (d).

from the stationary GP with the Gaussian kernel function:

$$\psi_\theta \left(t_i, t_j\right) = \exp\left(-\theta^2 \left(t_i - t_j\right)^2\right), \tag{24}$$

where θ is the smoothness (length-scale) parameter. A larger θ indicates a faster decay of temporal correlations in the signals. For CBNP signals, the power of tests is the same as the false discovery rate (FDR). A test with a lower FDR indicates its better capability for discriminating between periodicity and correlation.

We first compare the performance of the MO, the T^2, Fisher's, and the T tests for various source signals generated with different smoothness parameters θ. The results are shown in Fig. 5 (a), where the signal length is set to 5000. From Fig. 5 (a), the FDR of the proposed MO test is consistently low, staying around the significance level α, whereas the other tests lead to much higher FDRs, especially when the smoothness parameter θ is small or moderate. A high FDR indicates that the test would incorrectly report some correlated signals as periodic, leading to a high false alarm rate for periodicity detection. Clearly, the MO test is more effective than the other tests in distinguishing between periodicity and correlation. The FDR of each test decreases as the smoothness parameter θ increases, because the GP signals become more like white Gaussian noise as θ increases.

Next, we conduct another simulation investigating the influence of SNR (ranging from

−10 dB to 0 dB) on the FDR. We add white Gaussian noise to the above CBNP signals, where the smoothness parameter and signal length are fixed at 0.3 and 5000, respectively. Results are shown in Fig. 5 (b). It is seen that the FDRs of all tests, except for the MO test, increase rapidly with the SNR and converge to 1 when the SNR is higher than 0 dB. This result again demonstrates the MO test can effectively discriminate between periodicity and correlation, even in the presence of strong noise.

To study the impact of signal length (ranging from 5000 to 11000) on the FDR, the SNR and smoothness parameter are fixed at −2 dB and 0.3, respectively. Fig. 5 (c) shows that the FDR of the MO test is substantially lower than those of the other tests whose powers are close to one. This further verifies the capability of the MO test for effectively identifying the true periodicity subject to the intervention of correlation.

Moreover, Fig. 5 (c) and (d) demonstrate that the MO test maintains a low FDR for detecting the CBNP signals under two different q values ($\lfloor l/10 \rfloor$ and $\lfloor l/20 \rfloor$). These two simulations further indicate that the MO test is not sensitive to the choice of q when applied to distinguish between periodic signals and CBNP signals.

5.3   Control Charts for Periodicity Monitoring

It is seen from all of the above simulations that the MO test is unlikely to reject the null hypothesis when the signals are white Gaussian or CBNP. In this part, we will illustrate the performance of the proposed T^2 test for further discrimination between white Gaussian and CBNP signals. In this simulation, the original signals satisfy the null hypothesis, thus allowing the application of the MO and T^2 control charts for periodicity monitoring. The proposed control charts are compared with the spectral control chart (Beneke et al., 1988) based on Fisher's test.

We randomly generate 600 independent epochs, each consisting of 5000 signal points. The control limits are determined by setting $\alpha = 0.001$. We consider three scenarios of different process conditions. The first case consists of 200 epochs, in which white Gaussian
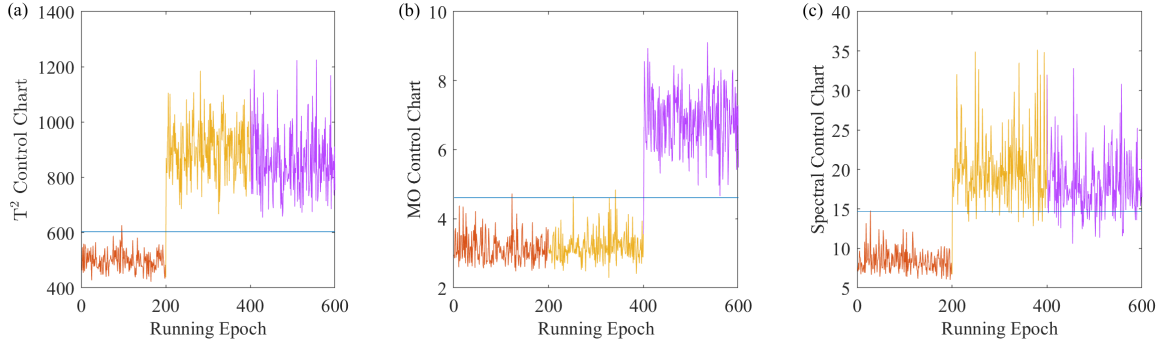
28

Figure 6: Control charts for three process conditions: (a) T^2 control chart, (b) MO control chart, and (c) spectral control chart.

noise is generated in each epoch. The second case consists of another 200 epochs, in which stationary GP signals are generated according to Eq. (24) with $\theta = 0.3$ and an SNR of 0 dB. In the last case of 200 epochs, periodic signals are generated according to Eq. (23), in which the SNR is set to -13 dB. Results are shown in Fig. 6, where these three scenarios are marked as red, yellow, and purple in the control charts, respectively. The control limit is represented by a horizontal blue line.

In Fig. 6, all three charts are in control for the first case (white Gaussian noise), because no cyclic behavior occurs in the process (marked by red color). For the second case (CBNP signals), the T^2 and spectral control charts are out of control, because most of the statistics marked as yellow exceed the control limit. By contrast, the MO control chart remains in control. For the third case (periodic signals), both the T^2 and MO control charts exhibit out-of-control behavior as anticipated, indicating their effectiveness in detecting periodicity. On the contrary, the spectral control chart occasionally fails to detect the periodic behavior.

In this simulation, it is clearly seen that none of the three control charts can discriminate the three cases all by itself. The MO control chart can effectively distinguish whether the signals are periodic, and the T^2 control chart can effectively discriminate whether the signals are white Gaussian. Therefore, we need to collaboratively consider both control charts. If both charts are in control, we can conclude that only white Gaussian noise is in
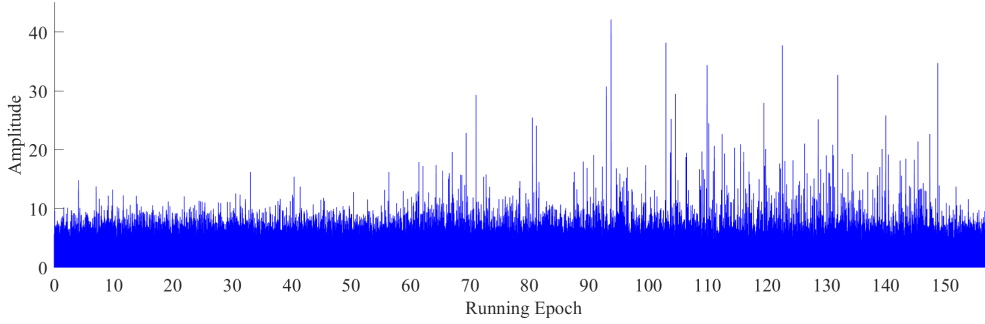
29

Figure 7: Bearing vibration signals of the run-to-failure experiment.

the process. If the MO chart is in control but the T^2 chart is out of control, the signals are CBNP. If the MO chart is out of control (we do not need to do T^2 chart in this case), we can conclude that periodic behaviors exist in the process.

6 Case Study

Rolling bearings are critical components in rotating machinery, and their reliability is important for maintaining product quality. Yet, they are susceptible to failure owing to many harsh operating conditions. When defects occur, the rolling elements of bearings produce periodic vibration signals (Li et al., 2023). In the early stage of failure, the periodic feature may be masked by complex background noise, making it challenging to detect. Thus, for timely maintenance and prevention of further damage, effective monitoring methods are needed to identify the periodicity (which is a sign of bearing fault) as early as possible.

To address this challenge, the proposed MO control chart is applied to the rolling bearing vibration signals for monitoring their health conditions. We consider the bearing run-to-failure datasets provided by the Institute of Design Science and Basic Component at Xi'an Jiaotong University (Wang et al., 2018); data are publicly available at https://biaowang.tech/xjtu-sy-bearing-datasets/. The vibration signals are recorded at a sampling frequency of 25.6 kHz in this bearing run-to-failure experiment. Every minute, 32,768 data points (1.28 s) are collected as one epoch. In this case study, we focus on the
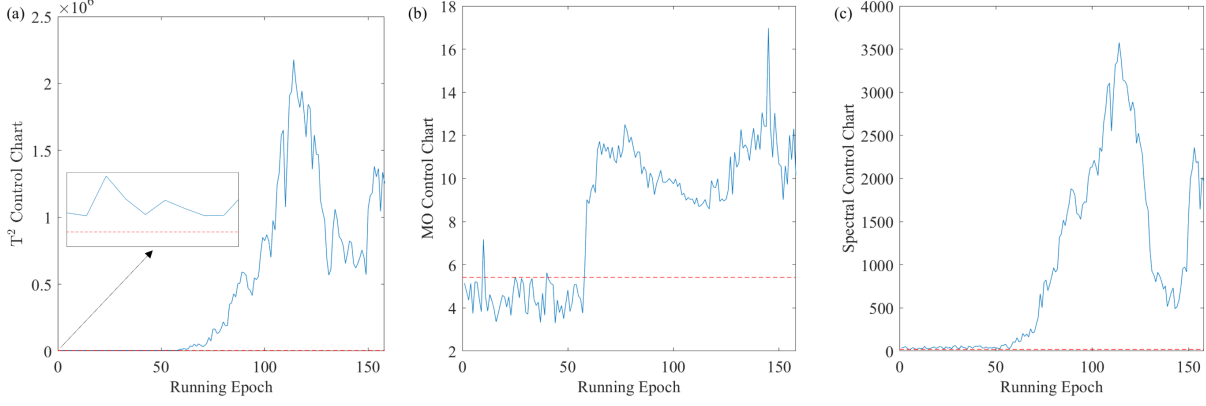
Figure 8: Control charts for the bearing case: (a) T^2 control chart, (b) MO control chart, and (c) spectral control chart.

vibration signals of bearings to monitor the degradation process. To validate our methods, we used the "bearing 1_3" dataset, which is reported to have an outer race fault in the experiment. There are 158 epochs in the target vibration signals, which are shown in Fig. 7. As indicated by these vibration signals, there should be no significant bearing fault observed before the 60th epoch.

We set the inspection period for the MO test from 2 to 3277, which is roughly 1/10 of the signal length in a single epoch. Subsequently, the MO control chart, along with the T^2 and spectral control charts, were applied to monitor the vibration signals, as illustrated in Fig. 8. The MO control chart exhibits almost no significant out-of-control events before the 60th epoch, although there were two alarm epochs. We suspect that the two alarms in the early stage are due to the use of an imperfect bearing in the run-to-failure experiment, which produces an extent of periodicity in the vibration signals. In contrast, both the T^2 and spectral control charts exceed their control limits from the initial stage, indicating the presence of correlation but no periodicity in the signals (i.e., the signals are CBNP) before the 60th epoch. All three control charts provided alarms after the 60th epoch, indicating that the bearing was likely to experience severe faults from that point onward. This is consistent with the onset of bearing faults during the end of the degradation experiment, as reported in Wang et al. (2018).
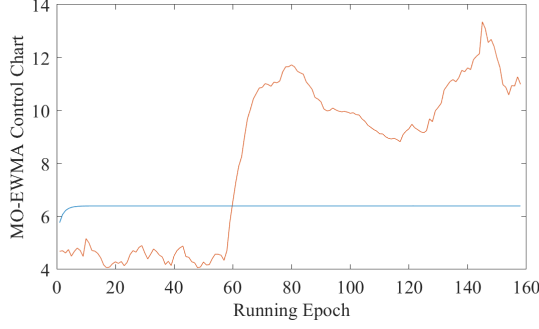
Figure 9: MO-EWMA control chart for the bearing dataset.

The MO control chart is effective in detecting the presence of periodicity in the bearing vibration signals, which is a sign of early bearing faults. However, in real production environments, it is often more critical to detect deviations in the bearing's working condition from its current state, particularly when we are not sure that the vibration signals satisfy the null hypothesis of the MO test. In such cases, the proposed MO-EWMA control chart better aligns with this practical need because it allows the monitoring of state changes (condition monitoring) without requiring its state to be purely white noises. The MO-EWMA control chart for the bearing dataset is shown in Fig. 9.

As observed, the EWMA control chart detected a noticeable change in the bearing's operating condition around the 60th epoch. The fault alarms generated by the MO-EWMA control chart are consistent with those generated by the MO control chart, indicating that the MO-EWMA control chart can achieve satisfactory performance in practical applications. It is worth noting that the MO-EWMA control chart, unlike the MO control chart, cannot determine when the periodicity has already emerged in the signals, but only indicates a deviation from the current state.

7   Conclusion

In this work, we first develop a new EnNRC feature to overcome the masking effect of strong noise in signal processing. Compared to the classic NRC, this new feature does not

suffer from unnecessary information loss and has appealing finite-sample and asymptotic properties (which cannot be found in NRC). Then, based on its theoretical properties, we propose the so-called MO and T^2 tests and construct their corresponding control charts. The MO control charts can accurately detect cyclic patterns from signals of a process under strong background noise. When used as a complement, the T^2 control charts can further distinguish between white Gaussian noises and CBNP signals. Notably, conventional spectral methods may be severely affected by strong noise and would erroneously report CBNP signals as periodic. The superiority of the proposed method has been illustrated via several numerical simulations. The bearing run-to-failure case study highlights its potential for process monitoring in real applications.

From the numerical examples, we can see that the proposed method exhibits remarkable efficiency in detecting cyclic trends in the process mean, but is less effective in detecting shifts in the process mean. When nonstationarity exists in the signals, it would be straightforward to complement our MO control chart with some conventional methods for detecting trends or shifts (Beneke et al., 1988), as Shewhart, CUSUM, and EWMA charts (Shewhart, 1931; Page, 1954; Roberts, 1959). When using the T^2 test (control chart) after the MO test (control chart) to discriminate CBNP signals, the inherent uncertainty of the the MO test (control chart) may introduce a potential bias into the critical value (control limit) of the T^2 test. To mitigate the risk of such a bias, we suggest using a two-stage FDR control (Benjamini and Hochberg, 1995; Wasserman, 2014) as a solution when combining these two test (control chart) methods sequentially. In addition, our approach may need relatively long signals (though much shorter compared to those required by the conventional methods) to eliminate the masking effect of very strong background noise, and thus it may become less effective for very short signal series. Nevertheless, this problem can be mitigated in practice by increasing the sampling frequency.

Another potential limitation of this work is that we only consider one common type of CBNP signals, i.e., signals generated from stationary GPs, but there are other types of

correlated signals in practice. We will further explore this problem in our planned future research. Furthermore, relaxing the assumption of white Gaussian noise and extending the proposed method beyond white Gaussian noises remains a challenging task for future research. Moreover, our methods could be extended to detect periodicity in functional time series inspired by Kokoszka et al. (2018) and Cerovecki et al. (2022), which is a promising direction for future research. Additionally, periodicity detection and monitoring of graphical data are also of interest in fields. The proposed methods could be applied to such applications in image and signal processing, which is another direction of our future work.

References

Austin, E., Eckley, I. A., and Bardwell, L. (2024), "Detection of Emergent Anomalous Structure in Functional Data," *Technometrics*, 1–11.

Beneke, M., Leemis, L. M., Schlegel, R. E., and Foote, B. L. (1988), "Spectral analysis in quality control: a control chart based on the periodogram," *Technometrics*, 30, 63–70.

Benjamini, Y. and Hochberg, Y. (1995), "Controlling the false discovery rate: a practical and powerful approach to multiple testing," *Journal of the Royal statistical society: series B (Methodological)*, 57, 289–300.

Beslin, S. and Ligh, S. (1989), "Greatest common divisor matrices," *Linear Algebra and its Applications*, 118, 69–76.

Bølviken, E. (1983), "New tests of significance in periodogram analysis," *Scandinavian Journal of Statistics*, 1–9.

Caragea, P. C. and Smith, R. L. (2007), "Asymptotic properties of computationally efficient alternative estimators for a class of multivariate normal models," *Journal of Multivariate Analysis*, 98, 1417–1440.

Cerovecki, C., Characiejus, V., and Hörmann, S. (2022), "The maximum of the periodogram of a sequence of functional data," *Journal of the American Statistical Association*, 1–9.

Colosimo, B. M., Jones-Farmer, L. A., Megahed, F. M., Paynabar, K., Ranjan, C., and Woodall, W. H. (2024), "Statistical Process Monitoring from Industry 2.0 to Industry 4.0: Insights into Research and Practice," *Technometrics*, 1–24.

Cramér, H. and Wold, H. (1936), "Some theorems on distribution functions," *Journal of the London Mathematical Society*, 1, 290–294.

Fan, W., Chen, Z., Li, Y., Zhu, F., and Xie, M. (2022), "A reinforced noise resistant correlation method for bearing condition monitoring," *IEEE Transactions on Automation Science and Engineering*, 20, 995–1006.

Fan, W., Jiang, F., Li, Y., and Peng, Z. (2024), "A Hankel Matrix-Based Multivariate Control Chart With Shrinkage Estimator for Condition Monitoring of Rolling Bearings," *IEEE Transactions on Automation Science and Engineering*.

Fan, W., Li, Y., Tsui, K. L., and Zhou, Q. (2018), "A noise resistant correlation method for period detection of noisy signals," *IEEE Transactions on Signal Processing*, 66, 2700–2710.

Fisher, R. A. (1929), "Tests of significance in harmonic analysis," *Proceedings of the Royal Society of London. Series A, Containing Papers of a Mathematical and Physical Character*, 125, 54–59.

Fuller, W. A. (2009), *Introduction to statistical time series*, John Wiley & Sons.

Genton, M. G. and Hall, P. (2007), "Statistical Inference for Evolving Periodic Functions," *Journal of the Royal Statistical Society Series B: Statistical Methodology*, 69, 643–657.

Hong, Y. (1996), "Consistent testing for serial correlation of unknown form," *Econometrica: Journal of the Econometric Society*, 837–864.

Hotelling, H. (1947), "Multivariate quality control-illustrated by the air testing of sample bombsights," *Techniques of Statistical Analysis*, 111–184.

Hurd, H. L. and Gerr, N. L. (1991), "Graphical methods for determining the presence of periodic correlation," *Journal of Time Series Analysis*, 12, 337–350.

Kokoszka, P., Nisol, G., et al. (2018), "Testing for periodicity in functional time series," *Annals of statistics*, 46.

Li, Y., Pu, Y., Cheng, C., and Xiao, Q. (2023), "A Scalable Gaussian Process for Large-Scale Periodic Data," *Technometrics*, 1–27.

Li, Y., Zhao, H., Fan, W., and Shen, C. (2021), "Generalized autocorrelation method for fault detection under varying-speed working conditions," *IEEE Transactions on Instrumentation and Measurement*, 70, 1–11.

Li, Y., Zhou, Q., Huang, X., and Zeng, L. (2018), "Pairwise estimation of multivariate gaussian process models with replicated observations: Application to multivariate profile monitoring," *Technometrics*, 60, 70–78.

McSweeney, L. (2006a), "Monitoring paper production using a spectral control chart designed to detect in the presence of multiple cycles," *Journal of Applied Statistics*, 33, 467–480.

McSweeney, L. A. (2006b), "Comparison of periodogram tests," *Journal of Statistical Computation and Simulation*, 76, 357–369.

Montgomery, D. C. (2019), *Introduction to statistical quality control*, John wiley & sons.

Moshrefzadeh, A. and Fasana, A. (2018), "The Autogram: An effective approach for selecting the optimal demodulation band in rolling element bearings diagnosis," *Mechanical systems and signal processing*, 105, 294–318.

Page, E. S. (1954), "Continuous inspection schemes," *Biometrika*, 41, 100–115.

Qiu, P. (2014), *Introduction to statistical process control*, CRC press.

Qiu, P., Li, W., and Li, J. (2020), "A new process control chart for monitoring short-range serially correlated data," *Technometrics*, 62, 71–83.

Rabiner, L. (1977), "On the use of autocorrelation analysis for pitch detection," *IEEE Transactions on acoustics, speech, and signal processing*, 25, 24–33.

Roberts, S. (1959), "Control chart tests based on geometric moving averages," *Technometrics*, 1, 239–250.

Shewhart, W. A. (1931), *Economic control of quality of manufactured product*, Macmillan And Co Ltd, London.

Shi, J. (2006), *Stream of variation modeling and analysis for multistage manufacturing processes*, CRC press.

Spurrier, J. D. and Thombs, L. (1990), "Control charts for detecting cyclical behavior," *Technometrics*, 32, 163–171.

Tatum, L. G. (1996), "Control charts for the detection of a periodic component," *Technometrics*, 38, 152–160.

Wang, B., Lei, Y., Li, N., and Li, N. (2018), "A hybrid prognostics approach for estimating remaining useful life of rolling element bearings," *IEEE Transactions on Reliability*, 69, 401–412.

Wasserman, L. (2014), *All of Statistics*, Springer.

Xie, X. and Qiu, P. (2024), "A general framework for robust monitoring of multivariate correlated processes," *Technometrics*, 66, 40–54.

Zhang, K., Bui, A. T., and Apley, D. W. (2023), "Concept drift monitoring and diagnostics of supervised learning models via score vectors," *Technometrics*, 65, 137–149.

Zhao-Guo, C. (1988), "Consistent estimates for hidden frequencies in a linear process," *Advances in applied probability*, 20, 295–314.

Zheng, Z., Ye, H., and Liu, K. (2024), "Online nonparametric monitoring for asynchronous processes with serial correlation," *IISE Transactions*, 1–14.

Zou, Q., Li, J., Ding, D., and Tsung, F. (2024), "Process monitoring for covariance matrices with latent structures," *IISE Transactions*, 1–12.

Appendix

1. *According to Eq. (21), we have*

$$l^2 \mathrm{Tr}\left(\boldsymbol{C}_i \boldsymbol{C}_j\right) = l^2 e_{[i,j]} \left(e_{[i,j]} - 1\right) \left(\boldsymbol{d}_{[i,j]}^i\right)^T \boldsymbol{d}_{[j,i]}^j + 2l^2 e_{[i,j]} \left(\boldsymbol{o}_{[i,j]}^i\right)^T \boldsymbol{o}_{[j,i]}^j.$$

Given that the maximum and minimum elements of $\boldsymbol{d}_{[i,j]}^i$ are $1/\left(e_i - 1\right)$ and $1/\left(o_i - 1\right)$ respectively, where o_i and e_i are defined in a similar way to o_n and e_n, we have

$$\frac{[i,j]}{(o_i - 1)(o_j - 1)} \leq l^2 \left(\boldsymbol{d}_{[i,j]}^i\right)^T \boldsymbol{d}_{[j,i]}^j \leq \frac{[i,j]}{(e_i - 1)(e_j - 1)},$$

by noting that $[i,j]$ is the length of $\boldsymbol{d}_{[i,j]}^i$ or $\boldsymbol{d}_{[j,i]}^j$. As $l \to \infty$, we have

$$\frac{[i,j]e_{[i,j]} \left(e_{[i,j]} - 1\right)}{(o_i - 1)(o_j - 1)} \to \frac{ij}{[i,j]}$$

because $e_{[i,j]}/o_i \to i/[i,j]$ and $e_{[i,j]}/o_j \to j/[i,j]$. Similarly, we also have

$$\frac{[i,j]e_{[i,j]} \left(e_{[i,j]} - 1\right)}{(e_i - 1)(e_j - 1)} \to \frac{ij}{[i,j]}.$$

The above two equations imply that

$$l^2 e_{[i,j]} \left(e_{[i,j]} - 1\right) \left(\boldsymbol{d}_{[i,j]}^i\right)^T \boldsymbol{d}_{[j,i]}^j \to (i,j),$$

given that $(i,j) = \frac{ij}{[i,j]}$. Recall that $\boldsymbol{o}_{[i,j]}^i$ is a subset of $\boldsymbol{d}_{[i,j]}^i$, so

$$\left(\boldsymbol{o}_{[i,j]}^i\right)^T \boldsymbol{o}_{[j,i]}^j < \left(\boldsymbol{d}_{[i,j]}^i\right)^T \boldsymbol{d}_{[j,i]}^j;$$

and thus

$$0 < l^2 e_{[i,j]} \left(\boldsymbol{o}_{[i,j]}^i\right)^T \boldsymbol{o}_{[j,i]}^j < \frac{e_{[i,j]}[i,j]}{(e_i - 1)(e_j - 1)} \to 0,$$

which means that $l^2 e_{[i,j]} \left(\boldsymbol{o}_{[i,j]}^i \right)^T \boldsymbol{o}_{[j,i]}^j \to 0$ as $l \to \infty$. Therefore,

$$l^2 \mathrm{Tr}\left(\boldsymbol{C}_i \boldsymbol{C}_j \right) = l^2 e_{[i,j]} \left(e_{[i,j]} - 1 \right) \left(\boldsymbol{d}_{[i,j]}^i \right)^T \boldsymbol{d}_{[j,i]}^j + 2l^2 e_{[i,j]} \left(\boldsymbol{o}_{[i,j]}^i \right)^T \boldsymbol{o}_{[j,i]}^j \to (i,j).$$

This completes the proof.

2. *According to the theorems in Caragea and Smith (2007), the sufficient condition of the asymptotic normality in Eq. (10) is*

$$\frac{\max_{k \leq l} \sum_{i=1}^{l} \sigma^4 \left(c_{i,k}^{(n)} \right)^2}{\mathsf{V}\left(\mathcal{C}_\epsilon (n) \right)} = \frac{\max_{k \leq l} \sum_{i=1}^{l} \left(c_{i,k}^{(n)} \right)^2}{2\mathrm{Tr}\left(\boldsymbol{C}_n \boldsymbol{C}_n \right)} \to 0,$$

as $l \to \infty$, where $c_{i,k}^{(n)}$ is the (i,k)th element of the matrix $\boldsymbol{C}_n$. Because $\frac{1}{e_n - 1} \geq \frac{1}{o_n - 1}$ for any n, we have

$$\max_{k \leq l} \sum_{i=1}^{l} \left(c_{i,k}^{(n)} \right)^2 \leq \frac{1}{l^2} \left(\frac{1}{e_n - 1} + \frac{1}{o_n - 1} \right) \leq \frac{2}{l^2 \left(e_n - 1 \right)}$$

and

$$\mathrm{Tr}\left(\boldsymbol{C}_n \boldsymbol{C}_n \right) = \frac{1}{l^2} \left(\frac{o_n n_1}{(o_n - 1)} + \frac{e_n n_2}{(e_n - 1)} \right) \geq \frac{1}{l \left(o_n - 1 \right)}.$$

Because $\frac{o_n - 1}{e_n - 1} \to 1$ as $l \to \infty$, we have

$$\frac{\max_{k \leq l} \sum_{i=1}^{l} \left(c_{i,k}^{(n)} \right)^2}{2\mathrm{Tr}\left(\boldsymbol{C}_n \boldsymbol{C}_n \right)} \leq \frac{\frac{2}{l^2 (e_n - 1)}}{\frac{2}{l (o_n - 1)}} = \frac{o_n - 1}{l \left(e_n - 1 \right)} \to 0.$$

This completes the proof.

3. *According to the theorems in Caragea and Smith (2007), the sufficient condition of the*

asymptotic normality in Eq. (11) is

$$\frac{\max_{k \leq l} \sum_{i=1}^{l} \sigma^4 \left(c_{i,k}^{(p)} - \sum_{n=1}^{p-1} \alpha_n c_{i,k}^{(n)} \right)^2}{\mathsf{V} \left(\mathcal{C}_\epsilon(p) - \sum_{n=1}^{p-1} \alpha_n \mathcal{C}_\epsilon(n) \right)} = \frac{\max_{k \leq l} \sum_{i=1}^{l} \left(c_{i,k}^{(p)} - \sum_{n=1}^{p-1} \alpha_n c_{i,k}^{(n)} \right)^2}{2\mathrm{Tr}\left(\left(\boldsymbol{C}_p - \sum_{n=1}^{p-1} \alpha_n \boldsymbol{C}_n \right)^2 \right)} \to 0, \qquad (25)$$

as $l \to \infty$. *Because* $\frac{1}{e_n - 1} \geq \frac{1}{o_n - 1}$ *for any* n, *we have*

$$\max_{k \leq l} \sum_{i=1}^{l} \left(c_{i,k}^{(p)} - \sum_{n=1}^{p-1} \alpha_n c_{i,k}^{(n)} \right)^2 \leq (r+1) \max_{k \leq l} \sum_{i=1}^{l} \left(\left(c_{i,k}^{(p)} \right)^2 + \sum_{n=1}^{p-1} \alpha_n^2 \left(c_{i,k}^{(n)} \right)^2 \right)$$

$$\leq \frac{r+1}{l^2} \left(\frac{1}{e_p - 1} + \sum_{n=1}^{p-1} \frac{\alpha_n^2}{e_n - 1} \right). \qquad (26)$$

The denominator of Eq. (25) can be rewritten as

$$2\mathrm{Tr}\left(\left(\boldsymbol{C}_p - \sum_{n=1}^{p-1} \alpha_n \boldsymbol{C}_n \right)^2 \right) = 2\boldsymbol{\omega}^T \boldsymbol{\Sigma}_l \boldsymbol{\omega},$$

where $\boldsymbol{\omega} = [-\alpha_1, \cdots, -\alpha_{p-1}, 1]^T$. *According to Theorem 1,* $l^2 \boldsymbol{\Sigma}_l$ *converges to a constant matrix* $\boldsymbol{\Sigma}$ *as* l *goes to infinity. Theorem 2 further implies that* $\boldsymbol{\omega}^T \left(l^2 \boldsymbol{\Sigma}_l \right) \boldsymbol{\omega}$ *is non-zero and will not converge to zero because* $\boldsymbol{\Sigma}_l$ *and* $\boldsymbol{\Sigma}$ *are strictly positive definite. Therefore, Eq. (26) implies that*

$$\frac{\max_{k \leq l} \sum_{i=1}^{l} \left(c_{i,k}^{(p)} - \sum_{n=1}^{p-1} \alpha_n c_{i,k}^{(n)} \right)^2}{2\mathrm{Tr}\left(\left(\boldsymbol{C}_p - \sum_{n=1}^{p-1} \alpha_n \boldsymbol{C}_n \right)^2 \right)} \leq \frac{(r+1)\left(1 + \sum_{n=1}^{p-1} \frac{(e_p-1)\alpha_n^2}{e_n-1} \right)}{2(e_p-1)\boldsymbol{\omega}^T \left(l^2 \boldsymbol{\Sigma}_l \right) \boldsymbol{\omega}} \leq \frac{(r+1)\left(1 + \sum_{n=1}^{p-1} \alpha_n^2 \right)}{2(e_p-1)\boldsymbol{\omega}^T \left(l^2 \boldsymbol{\Sigma}_l \right) \boldsymbol{\omega}} \to 0$$

because $\boldsymbol{\omega}^T \left(l^2 \boldsymbol{\Sigma}_l \right) \boldsymbol{\omega}$ *converges to a non-zero constant and* $e_p \to \infty$ *as* $l \to \infty$. *This convergence indicates that the sufficient condition in Eq. (25) is satisfied. This completes the*

proof.

1. *We only consider the case when $l \% n \neq 0$, and the proof under the case when $l \% n = 0$ is omitted here because it is quite similar to and much simpler than the proof under the case when $l \% n \neq 0$. The inequality $\|C_n x\| \leq \|x\| / l$ is first proved by utilizing the Cauchy-Schwarz inequality because*

$$
\begin{aligned}
\|C_n x\|^2 &= \sum_{i=1}^{o_n} \left(O_n \sum_{j=1,j\neq i}^{o_n} x_{j,1} \right)^2 + \sum_{i=1}^{e_n} \left(E_n \sum_{j=1,j\neq i}^{e_n} x_{j,2} \right)^2 \\
&= \frac{\sum_{i=1}^{o_n} \left\| \sum_{j=1,j\neq i}^{o_n} \frac{x_{j,1}}{o_n - 1} \right\|^2 + \sum_{i=1}^{e_n} \left\| \sum_{j=1,j\neq i}^{e_n} \frac{x_{j,2}}{e_n - 1} \right\|^2}{l^2} \\
&\leq \frac{\sum_{i=1}^{o_n} \sum_{j=1,j\neq i}^{o_n} \frac{\|x_{j,1}\|^2}{o_n - 1} + \sum_{i=1}^{e_n} \sum_{j=1,j\neq i}^{e_n} \frac{\|x_{j,2}\|^2}{e_n - 1}}{l^2} \\
&= \frac{\sum_{i=1}^{o_n} \|x_{i,1}\|^2 + \sum_{i=1}^{e_n} \|x_{i,2}\|^2}{l^2} = \frac{\|x\|^2}{l^2},
\end{aligned}
$$

for any $n < l/2$, and the equality holds if and only if $x_{i,1} = x_{j,1}$ and $x_{i,2} = x_{j,2}$ for all i, j. That is, the equality $\|C_n x\| = \|x\| / l$ holds if and only if the signal x is periodic, and its period p_0 should be divided by n, i.e., $n \in \mathbb{N}$. We also have

$$
x^T C_n x \leq \|x\| \|C_n x\| \leq \|x\|^2 / l
$$

for any x because $\|C_n x\| \leq \|x\| / l$, and the equality holds if and only if $\|C_n x\| = \|x\| / l$. Therefore, the sufficient and necessary condition of $x^T C_n x = \|x\|^2 / l$ is that x is periodic and $n \in \mathbb{N}$. This completes the proof.

2. *We first prove that Σ_l is positive semidefinite when $l > p + 1$. Recall that the ith and jth element of Σ_l is $\text{Tr}(C_i C_j) = (\text{Vec}(C_i))^T \text{Vec}(C_j)$, which indicates that Σ_l can be*

41

decomposed into the product of two matrices:

$$\boldsymbol{\Sigma}_l = \boldsymbol{A}_l^T \boldsymbol{A}_l,$$

where $\boldsymbol{A}_l = [\text{Vec}(\boldsymbol{C}_1), \text{Vec}(\boldsymbol{C}_2), \cdots, \text{Vec}(\boldsymbol{C}_p)]$. This decomposition means that $\boldsymbol{\Sigma}_l$ is positive semidefinite.

Then, we prove that $\boldsymbol{A}_l$ is column full rank. According to the definition of $\boldsymbol{C}_n$, we have

$$\boldsymbol{A}_l = \begin{bmatrix} 0 & 0 & \cdots & 0 & 0 \\ \frac{1}{(o_1-1)l} & 0 & \cdots & 0 & 0 \\ \vdots & \frac{1}{(o_2-1)l} & \ddots & \ddots & \vdots \\ * & * & \cdots & \frac{1}{(o_{p-1}-1)l} & 0 \\ * & * & \cdots & * & \frac{1}{(o_p-1)l} \\ \vdots & \vdots & \vdots & \vdots & \vdots \end{bmatrix}$$

when $l > p + 1$, where $*$ denotes the elements that are not interested. Thus, $\boldsymbol{A}_l$ is column full rank, which implies that $\boldsymbol{\Sigma}_l$ is positive definite. This completes the proof.

3. From Eq. (5), we have

$$\mathsf{V}\left(\mathcal{C}_{\boldsymbol{y}}(n)\right) = 2\sigma^4 \text{Tr}\left(\boldsymbol{C}_n \boldsymbol{C}_n\right) + 4\sigma^2 \boldsymbol{x}^T \boldsymbol{C}_n \boldsymbol{C}_n \boldsymbol{x},$$

where

$$\text{Tr}\left(\boldsymbol{C}_n \boldsymbol{C}_n\right) = \frac{1}{l^2}\left(\frac{o_n n_1}{(o_n - 1)} + \frac{e_n n_2}{(e_n - 1)}\right),$$

which implies that $\text{Tr}\left(\boldsymbol{C}_n \boldsymbol{C}_n\right) \to 0$ as $l \to \infty$. According to the proof for Theorem 1, we have $\|\boldsymbol{C}_n \boldsymbol{x}\| \le \|\boldsymbol{x}\|/l$, and thus,

$$\boldsymbol{x}^T \boldsymbol{C}_n \boldsymbol{C}_n \boldsymbol{x} = \|\boldsymbol{C}_n \boldsymbol{x}\|^2 \le \|\boldsymbol{x}\|^2/l^2 = \frac{\mathcal{P}_{\boldsymbol{x}}}{l} \to 0, \text{ as } l \to \infty.$$

$\text{Tr}\left(\boldsymbol{C}_n \boldsymbol{C}_n\right) \to 0$ and $\boldsymbol{x}^T \boldsymbol{C}_n \boldsymbol{C}_n \boldsymbol{x} \to 0$ imply that $\mathsf{V}\left(\mathcal{C}_{\boldsymbol{y}}\left(n\right)\right) \to 0$ as $l \to \infty$, and hence

$$\mathsf{V}\left(\mathcal{C}_{\boldsymbol{y}}\left(n\right) - \mathcal{C}_{\boldsymbol{x}}\left(n\right)\right) = \mathsf{V}\left(\mathcal{C}_{\boldsymbol{y}}\left(n\right)\right) \to 0, \;\; as \; l \to \infty.$$

According to Chebyshev's inequality, for any $\epsilon > 0$,

$$\mathsf{P}\left(\left|\mathcal{C}_{\boldsymbol{y}}\left(n\right) - \mathcal{C}_{\boldsymbol{x}}\left(n\right)\right| > \epsilon\right) \leq \frac{\mathsf{V}\left(\mathcal{C}_{\boldsymbol{y}}\left(n\right) - \mathcal{C}_{\boldsymbol{x}}\left(n\right)\right)}{\epsilon^2} \to 0,$$

as $l \to \infty$. Therefore, $\mathcal{C}_{\boldsymbol{y}}\left(n\right) - \mathcal{C}_{\boldsymbol{x}}\left(n\right) \xrightarrow{p} 0, \;\; as \; l \to \infty$. This completes the proof.

4. *Lemmas 2 and 3 imply that*

$$\frac{\boldsymbol{\omega}^T \mathcal{C}_{\boldsymbol{\epsilon}}^{(1:p)}}{\sqrt{\mathsf{Var}\left(\boldsymbol{\omega}^T \mathcal{C}_{\boldsymbol{\epsilon}}^{(1:p)}\right)}} = \frac{\boldsymbol{\omega}^T \mathcal{C}_{\boldsymbol{\epsilon}}^{(1:p)}}{\sqrt{2\sigma^4 \boldsymbol{\omega}^T \boldsymbol{\Sigma}_l \boldsymbol{\omega}}} \xrightarrow{d} \mathcal{N}\left(0, 1\right)$$

for any $\boldsymbol{\omega}$ because $2\sigma^4 \boldsymbol{\Sigma}_l$ is the covariance matrix of $\mathcal{C}_{\boldsymbol{\epsilon}}^{(1:p)}$. Plugging Eq. (9) into the above equation results in

$$\boldsymbol{\omega}^T l \mathcal{C}_{\boldsymbol{\epsilon}}^{(1:p)} \xrightarrow{d} \mathcal{N}\left(\boldsymbol{0}, 2\sigma^4 \boldsymbol{\omega}^T \boldsymbol{\Sigma} \boldsymbol{\omega}\right)$$

for any $\boldsymbol{\omega}$. According to the Cramer-Wold theorem (Cramér and Wold, 1936), we have

$$l \mathcal{C}_{\boldsymbol{\epsilon}}^{(1:p)} \xrightarrow{d} \mathcal{N}\left(\boldsymbol{0}, 2\sigma^4 \boldsymbol{\Sigma}\right).$$

Next, we prove that $\boldsymbol{\Sigma}$ is positive definite. A periodic vector $\boldsymbol{a}_i$ is denoted by

$$\boldsymbol{a}_i = \left[0, \cdots, 0, \frac{i}{\sqrt{[1, \cdots, p]}}, \ldots, 0, \cdots, 0, \frac{i}{\sqrt{[1, \cdots, p]}}\right]^T,$$

which is a periodic vector with nonzero element $i/\sqrt{[1, \cdots, p]}$ at the ith position and its multiples, where $[1, \cdots, p]$ is the LCM of $1, 2, \cdots, p$. The definition of $\boldsymbol{a}_i$ implies that $\boldsymbol{a}_i^T \boldsymbol{a}_j$

equals to the ith and jthe element of $\boldsymbol{\Sigma}$ because

$$\boldsymbol{a}_i^T \boldsymbol{a}_j = \frac{[1, \cdots, p]}{[i, j]} \underset{\sqrt{[1, \cdots, p]}}{\overset{i}{}} \underset{\sqrt{[1, \cdots, p]}}{\overset{j}{}} = (i, j)$$

by noting that $ij/[i, j] = (i, j)$. Thus, $\boldsymbol{\Sigma}$ can be decomposed into the product of two matrices, i.e.,

$$\boldsymbol{\Sigma} = \boldsymbol{A}^T \boldsymbol{A},$$

where $\boldsymbol{A} = [\boldsymbol{a}_1, \boldsymbol{a}_2, \cdots, \boldsymbol{a}_p]$. This decomposition means that $\boldsymbol{\Sigma}$ is positive semidefinite. The matrix is column full rank because

$$\boldsymbol{A} = \frac{1}{\sqrt{[1, \cdots, p]}} \begin{bmatrix} 1 & 0 & \cdots & 0 & 0 \\ 1 & 2 & \cdots & 0 & 0 \\ 1 & 0 & \ddots & \vdots & \vdots \\ * & * & \cdots & p-1 & 0 \\ * & * & \cdots & * & p \\ \vdots & \vdots & \vdots & \vdots & \vdots \end{bmatrix}.$$

Therefore, the full rank matrix $\boldsymbol{A}$ guarantees $\boldsymbol{\Sigma}$ to be positive definite. This completes the proof.

5. According to Theorem 4, we have

$$\frac{\boldsymbol{\Sigma}_l^{-1/2} \mathcal{C}_{\boldsymbol{\epsilon}}^{(1:n)}}{\sqrt{2\sigma^2}} \xrightarrow{d} \mathcal{N}\left(\boldsymbol{0}, \boldsymbol{I}_{n \times n}\right),$$

by applying the continuous mapping theorem, where $\boldsymbol{\Sigma}_l^{-1/2} \boldsymbol{\Sigma}_l^{-1/2} = \boldsymbol{\Sigma}_l^{-1}$. Note that $\mathcal{C}_{\boldsymbol{y}}(p_1), \cdots, \mathcal{C}_{\boldsymbol{y}}(p_q)$ is a subset of $\mathcal{C}_{\boldsymbol{\epsilon}}^{(1:n)}$ when $n \geq p_q$, and thus

$$\frac{\boldsymbol{\Xi}_l^{-1/2}}{\sqrt{2\sigma^2}} \mathcal{C}_{\boldsymbol{y}} \xrightarrow{d} \mathcal{N}\left(\boldsymbol{0}, \boldsymbol{I}_{q \times q}\right),$$

which directly implies that T^2 follows a chi-square distribution asymptotically with q degrees of freedom, by utilizing the continuous mapping theorem, i.e.,

$$\mathrm{T}^2 \sim \chi^2\left(q\right).$$

This completes the proof.